

Enhanced methane flux event and sediment dispersal pattern in the Krishna–Godavari offshore basin: Evidences from rock magnetic techniques

A. Usapkar, P. Dewangan*, M. Kocherla, T. Ramprasad, A. Mazumdar, M.V. Ramana

CSIR-National Institute of Oceanography, Dona Paula, Goa, 403004, India



ARTICLE INFO

Article history:

Received 7 October 2013

Received in revised form

11 July 2014

Accepted 9 August 2014

Available online 19 August 2014

Keywords:

Magnetic dissolution

SMTZ

Methane flux

AOM

Sediment transport/sorting mechanism

ABSTRACT

Detailed rock magnetic measurements such as susceptibility (χ), susceptibility of anhysteretic remanent magnetization (X_{ARM}), saturation isothermal remanent magnetization (SIRM), soft-isothermal remanent magnetization (soft-IRM) and hard-IRM (HIRM) were carried out on the topmost sediment samples of 73 gravity cores collected in the Krishna–Godavari (KG) offshore basin to understand the distribution of magnetic parameters and the associated diagenetic signatures related to upward methane flux. The variation in magnetic parameters in the KG offshore basin fluctuates around the average value ($\chi = 105 \times 10^{-8} \text{ m}^3 \text{ kg}^{-1}$, $X_{ARM} = 1.22 \times 10^{-5} \text{ m}^3 \text{ kg}^{-1}$, $SIRM = 2040 \times 10^{-5} \text{ Am}^2 \text{ kg}^{-1}$, soft-IRM = 1807 and HIRM = 82) except at the location GC-07 (15.767°N, 81.814°E) where the magnetic parameters χ , X_{ARM} and SIRM drop to ~1/6th, ~1/14th and ~1/8th of the average near surface value indicating substantial loss in the concentration of primary magnetic iron oxide minerals. Anomalous low value of X_{ARM}/χ and $X_{ARM}/SIRM$ at GC-07 suggests that the magnetic remanence property is governed by coarser pseudo-single domain (PSD) or multi-domain (MD) grains. To understand the nature of the anomalous magnetic parameters at GC-07, complete downcore variation of magnetic parameters was also studied. The magnetic parameters were found to be even more depleted at all depths with susceptibility dropping (at 5.2 mbsf) to ~1/200th of its average near surface value. Interestingly, this core shows a rapid increase in the concentration of dissolved methane from ~0 nM at surface to ~153 nM at around 5.2 mbsf where the sulfate concentration is also reduced to zero. The anaerobic oxidation of methane (AOM) and the sulfate methane transition zone (SMTZ) occur between ~4.2 and 5.2 mbsf based on the present day sulfate concentration profile. The close association between the dissolution of magnetic iron oxide minerals and AOM at GC-07 suggests that the reduced magnetization is primarily due to the release of HS^- by AOM. The magnetic iron oxide minerals are dissolved not only at SMTZ but also above the current depth of the SMTZ. It is likely that the methane flux was higher in the past leading to upward shift of the SMTZ, and the HS^- released by AOM facilitated the dissolution of magnetic iron oxide minerals at shallower depths. Alternatively, the HS^- diffusing upward from the current depth of SMTZ might have led to dissolution at shallower depth. Therefore, additional geological/geochemical investigations are warranted at GC-07 to establish the dissolution mechanism of magnetic iron oxide minerals.

The variability in different magnetic parameters within the slope basin and channels shows systematic decrease in the concentration of magnetic minerals and increase in the abundance of stable single domain (SSD) magnetic grains with water depth. The observed strong correlation between the silt fraction and the magnetic susceptibility for the slope basin and channels suggests that the variation in magnetic parameters is predominantly controlled by the sediment sorting/transport process as finer particles are deposited in deeper water.

© 2014 Elsevier Ltd. All rights reserved.

1. Introduction

Magnetic parameters obtained in a rapid, non destructive manner, have been increasingly used as proxies for paleoclimate reconstruction (e.g. Thompson and Maher, 1995; Reynolds and

* Corresponding author.

E-mail address: pdewangan@nio.org (P. Dewangan).

King, 1995; Geiss and Banerjee, 1997; Tang et al., 2003), pale rainfall reconstruction (e.g. Maher et al., 1994; Maher and Thompson, 1995; Basavaiah and Khadkikar, 2004), pollution assessment (e.g. Hoffmann et al., 1999; Petrovský et al., 2000) and identification of sediment provenance and transport pathways (Thompson et al., 1975; Oldfield et al., 1985; Oldfield, 1991; Dearing, 2000; Duck et al., 2001; Booth et al., 2005; Rotman et al., 2008). In the recent past, magnetic properties have also been used as proxy indicators for the identification of methane venting zones. Magnetic anomalies associated with seepage regions are mapped either through aeromagnetic surveys or by systematic study of soil and sediment samples (Donovan et al., 1979; Schumacher, 1996; Liu et al., 2004a; Novosel et al., 2005; Riedel et al., 2006; Zhong et al., 2009; Esteban et al., 2010). Often, the hydrocarbon seepage (mostly methane gas) occurs in the region associated with gas hydrate and deeper oil/gas fields. Magnetic minerals are either precipitated or dissolved under the influence of hydrocarbons in a seep environment (Machel and Burton, 1991; Roberts et al., 2006; Rowan and Roberts, 2006; Fu et al., 2008). Depending on the background concentration of magnetic minerals, precipitation of authigenic magnetic minerals and dissolution of primary magnetic iron oxide minerals may lead to either enhancement or reduction in magnetic signatures associated with the seep. Many rock magnetic and geochemical studies have shown the enhancement of magnetic susceptibility and other magnetic parameters due to precipitation of authigenic magnetite/maghemite and metastable greigite in the methane/hydrocarbon seep environment (Donovan et al., 1979; Liu et al., 2004a, 2006) while others have shown the relationship with reduction in the concentration of magnetic iron oxide minerals, authigenic formation of iron sulfides, and occurrence of methane in marine sediments (Housen and Musgrave, 1996; Riedinger et al., 2005; Larrasoña et al., 2006; Musgrave et al., 2006; Larrasoña et al., 2007; Fu et al., 2008; März et al., 2008; Dewangan et al., 2013). The corresponding geochemical processes are discussed by Kasten et al. (1998), Neretin et al. (2004), Garming et al. (2005), Horng and Chen (2006). Due to the close association of methane flux with magnetic anomalies, rock magnetic techniques are used as a reliable tool for the identification and mapping of methane venting zones under different geological environments.

Magnetic parameters of surficial sediments can also be used to identify source and transport mechanism of sediments in the marine environment. A number of studies have used the magnetic variability of surface sediments for identifying sediment provenance and transport pathways (Thompson et al., 1975; Oldfield, 1991; Walden et al., 1997; Dearing, 2000; Duck et al., 2001; Booth et al., 2005; Rotman et al., 2008). Ellwood et al. (2006) used magnetic susceptibility and ARM measurements, and inferred the sediment source and flow pattern for the Gulf of Mexico sediments. Magnetic susceptibility of different grain size fractions, and its effect on sediment transport pathways and provenance have been further studied by Wang et al. (2009) for Changjiang and Huanghe estuaries, Liu et al. (2010) for south China Sea and Wang et al. (2010) for the north-eastern continental shelves of China. Therefore, it is evident that magnetic properties if used under the constraints of other sedimentological attributes can be effective in delineating subsurface geological environment.

The Krishna–Godavari (KG) offshore basin is a proven petrolierous basin of India, and the geoscientific investigations carried out onboard *R/V AAA Sidorenko* (2002–03) provided significant information on the nature of the sediments, their physical, chemical and microbial properties. Several surface and subsurface gas escape features mostly related to fluid/gas expulsion in the shallow sediments are mapped in this basin (NIO, 2005; Ramana et al., 2006, 2007; Dewangan et al., 2010). Based on the spatial distribution of gas escape features, 73 gravity cores of 1–5 m long were collected

in the water depths ranging from 670 to 1745 m (NIO, 2005) in the study area. The downcore variation of pore water sulfate, methane flux, and the inferred sulfate–methane transition zone at several locations are reported (NIO, 2005; Mazumdar et al., 2007, 2012). Methane-derived authigenic carbonates with highly depleted carbon isotopic ratio within the subsurface sediments have been observed indicating upward migration/seepage of methane in the study area (Mazumdar et al., 2009, 2012; Dewangan et al., 2013). Detailed rock magnetic measurements of a ~30 m long core (MD161-8) in KG offshore basin established the link between the diagenesis of magnetic iron oxide minerals and paleo-methane seepage (Dewangan et al., 2013). However, magnetic variability and its possible linkage to methane venting/gas hydrate have not been studied on these spatially distributed sediment cores in KG offshore basin. Therefore, we carried out detailed magnetic measurements of the topmost sediment samples of 73 gravity cores and attempted to understand the magnetic signatures associated with upward methane flux and the sediment transport/sorting process which governs the variability of these magnetic parameters.

2. Geological settings

The Krishna–Godavari (KG) basin, a pericratonic rift basin (Rao, 2001), lies in the middle of the eastern continental margin of India (ECMI) which evolved after the break up of Gondwanaland around 130 Ma years ago (Powell et al., 1988; Scotese et al., 1988; Ramana et al., 1994). The basin extends ~28,000 km² onshore and ~145,000 km² offshore. Much of the detrital influx in KG basin is brought by Krishna and Godavari, the two major river systems. The sediment thickness ranges from 3 to 5 km in the onshore region to ~8 km in the offshore region (Prabhakar and Zutshi, 1993; Bastia, 2007). The sediment in the study area consists of silty clay with a negligible amount of sand fraction (NIO, 2005). The dominant clay fraction is montmorillonite with traces of illite and kaolinite.

In the KG offshore basin, widespread presence of gas hydrate is inferred from the bottom-simulation reflections (BSRs) on the seismic data. Drilling/coring in this basin has confirmed the presence of subsurface gas hydrate deposits (Collett et al., 2008). Several acoustic features related to fluid/gas migration have been reported in the shallow subsurface (Ramana et al., 2007, 2009; Dewangan et al., 2010) supported by geochemical evidence (Mazumdar et al., 2009) which confirms active migration of methane and presence of paleo seeps. Further, slumping/sliding of slope sediments, associated with fluid/gas migration has led to several mass transport deposits (Rampasad et al., 2011). Several bathymetry mounds formed due to shale tectonics/neo-tectonics are heavily faulted, and show acoustic signatures of fluid/gas migration through the fault system (Dewangan et al., 2010). The analysis of available geophysical datasets such as multi-channel seismic, high resolution seismic, sub-bottom profiler and multibeam bathymetry has divided the study area into distinct geological/depositional environments (Fig. 1) such as a mid-slope mini-basin, two channel like features in the north-east (NE) and south-west (SW) directions, bathymetry mounds, toe-thrust sedimentary ridges and deep ocean basin (Ramana et al., 2007, 2009; Dewangan et al., 2010; Rampasad et al., 2011).

3. Sampling and methods

In the KG offshore basin, 73 gravity cores, ~5 m long, were collected under the gas hydrate exploration program (Fig. 1). After the core retrieval, the top 2 cm of the core were scooped and transferred into clean plastic vials avoiding any magnetic contamination. Generally, the top few centimeters of sediment is lost during gravity coring, therefore, these samples may not represent the surface sediments and will be referred to as the topmost

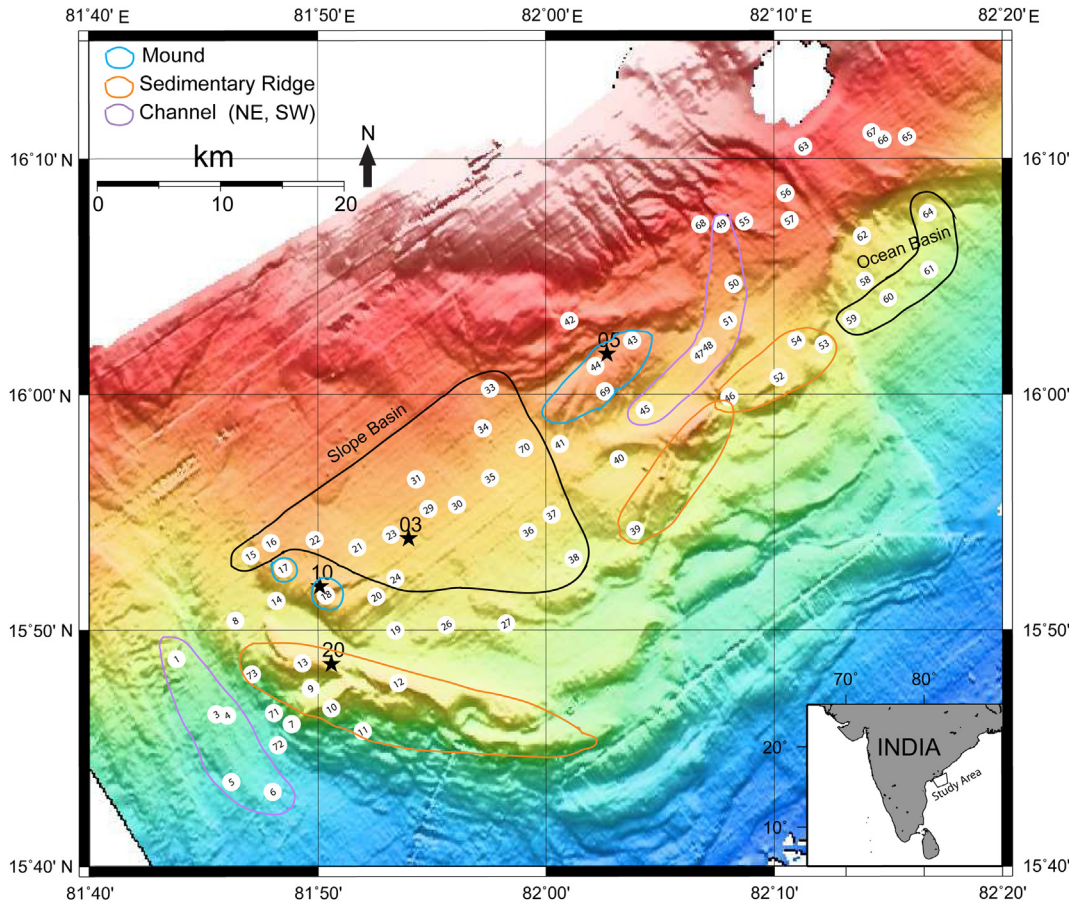


Figure 1. Location map of the study area in Krishna–Godavari offshore basin. The inset shows the zoom out of the study area. Circles with numbers represent locations of the GC cores. Black stars represent locations of the NGHP-Expedition-01.

sediment samples. About 10 g of topmost sediment samples were oven dried at 40 °C for 24 h for magnetic measurements (Collinson, 1983). Dried samples were crushed gently to disintegrate the grains. It was weighed and packed in 7 cm³ cylindrical plastic sampling bottles using a clean wrap for magnetic measurements. The weight of the samples was obtained for normalization of magnetic measurements after accounting for the weight of the sampling bottle and clean wrap.

The samples were analyzed for mass dependent magnetic susceptibility using a Bartington MS2B dual frequency susceptibility meter. Measurements were done at two different frequencies, low frequency susceptibility $X_{LF} = 0.47$ kHz and high frequency susceptibility $X_{HF} = 4.7$ kHz, and the frequency dependent magnetic susceptibility was calculated using, $X_{FD} (\%) = [(X_{LF} - X_{HF})/X_{LF}] \times 100$; X_{LF} will be referred to as magnetic susceptibility (X). Subsequently, the samples were subjected to anhysteretic remanent magnetization (ARM) measurements. The sample was exposed to a fixed DC bias field of 50 µT on a peak alternating field of 100 mT using AF-demagnetizer. The imparted ARM was measured using a Molspin fluxgate spinner magnetometer and was normalized by sample weight. The susceptibility of ARM i.e. X_{ARM} was calculated using the formula $X_{ARM} = ARM/DC$ bias field. Isothermal remanent magnetism (IRM) was imparted using a pulse magnetizer MMP10 at a forward field of 1T and then backward fields of –20 mT, –30 mT, –100 mT and –300 mT, and remnant magnetization was measured using Molspin fluxgate spinner magnetometer. The S-ratio (Thompson and Oldfield, 1986; Bloemendal et al., 1988) was calculated as IRM_{-300mT}/IRM_{1T} . Soft and hard-IRM (HIRM) were calculated using the formulas: soft-IRM = $(IRM_{1T} - (IRM_{-30mT}))/(sample\ weight)$ and HIRM = $(IRM_{1T} - (IRM_{-300mT}))/(sample\ weight)$. $IRM_{1T}/(sample\ weight)$ is considered as saturation isothermal remanent magnetization (SIRM). Although freeze drying is recommended for the magnetic measurements to avoid thermal effect on the magnetic properties and oxidation of finer magnetic particles, our laboratory tests suggest that oven drying may lead to <10% reduction in X_{ARM} with negligible effect on magnetic susceptibility and other IRM measurements.

The magnetic particles from GC-07 and nearby cores GC-09 and GC-72 were extracted from the slurry of sediments. The slurry was made to pass over a gently inclined aluminum C-channel (8" wide and 28" long) placed above a strong permanent 1T magnet. After the removal of the strong magnet, the particles attached to the C-channel were cleaned using distilled water. Images of this extract were captured using an SEM (JEOL JSM-5800LV) and its elemental analysis was carried out using an energy dispersive X-ray spectroscopy (EDS). Grain size analyses were carried out by standard gravitational settling method (Tucker, 1988).

4. Results

The variability of magnetic parameters of the topmost sediment samples is studied in the KG offshore basin (Table 1). Average value and standard deviation of magnetic parameters is shown in Table 2 for all samples except GC-07. The location GC-07 shows a prominent reduction in susceptibility, X_{ARM} and SIRM values as compared to the average near surface values.

The magnetic susceptibility (Fig. 2A) within the slope basin, NE and SW channels decreases systematically with depth. Higher

Table 1

Magnetic and silt variability for surface samples of GC cores from K-G offshore basin.

Core ID	Latitude	Longitude	Water depth (m)	Core length (m)	χ ($\times 10^{-8} \text{ m}^3 \text{ kg}^{-1}$)	χ_{ARM} ($\times 10^{-5} \text{ m}^3 \text{ kg}^{-1}$)	SIRM ($\times 10^{-5} \text{ Am}^2 \text{ kg}^{-1}$)	Soft-IRM	HIRM	S-ratio	Silt (%)
GH4/GC-63	16.175	82.188	671	4.2	98.17	1.23	1872.37	1667.69	83.88	0.955	21.06
GH4/GC-68	16.120	82.113	782	4.8	105.91	1.28	2048.27	1739.16	65.67	0.968	17.1
GH4/GC-42	16.052	82.017	783	3.7	91.83	1.17	1704.07	1540.62	69.30	0.959	31.89
GH4/GC-49	16.120	82.128	786	4.5	125.66	1.30	2582.29	2243.55	23.20	0.991	34.68
GH4/GC-67	16.185	82.238	794	4.2	88.65	1.17	1627.21	1372.37	37.51	0.977	27.49
GH4/GC-55	16.122	82.145	802	4	107.64	1.20	2171.92	1942.73	39.02	0.982	27.8
GH4/GC-56	16.142	82.175	819	4.2	95.18	1.24	1816.85	1672.39	85.99	0.953	26.68
GH4/GC-66	16.180	82.246	819	4.2	95.85	1.20	1812.42	1611.27	79.41	0.956	32.5
GH4/GC-65	16.182	82.264	871	3.9	122.53	1.27	2422.96	2009.28	108.52	0.955	25.97
GH4/GC-57	16.123	82.178	879	4.2	113.47	1.29	2278.10	2092.82	100.43	0.956	24.9
GH4/GC-43	16.038	82.063	927	3.9	97.71	1.20	1788.76	1562.71	106.85	0.940	23.81
GH4/GC-33	16.004	81.959	951	4.4	122.05	1.23	2409.06	2014.83	97.58	0.959	30.76
GH4/GC-44	16.020	82.036	951	4.1	98.48	1.25	1799.29	1653.90	66.33	0.963	26.48
GH4/GC-50	16.078	82.137	961	4.7	115.57	1.16	2422.48	2143.88	100.53	0.959	28.58
GH4/GC-69	16.002	82.043	980	4.7	91.29	1.12	1711.11	1515.38	87.98	0.949	21.19
GH4/GC-34	15.976	81.954	996	4	118.56	1.26	2310.16	2024.41	80.79	0.965	26.22
GH4/GC-31	15.940	81.905	1000	4.3	115.61	1.22	2243.61	1937.70	86.05	0.962	35.04
GH4/GC-16	15.895	81.799	1004	3.9	116.01	1.25	2202.17	1949.22	71.40	0.968	24.74
GH4/GC-22	15.897	81.831	1017	3.5	121.18	1.23	2549.14	2362.74	57.84	0.977	26.09
GH4/GC-51	16.052	82.133	1022	3.5	116.61	1.19	2147.88	1899.38	116.63	0.946	30.45
GH4/GC-48	16.034	82.118	1023	4	116.49	1.28	2245.60	1974.84	52.66	0.977	24.2
GH4/GC-47	16.028	82.112	1033	4.2	109.06	1.34	2067.68	1812.65	74.65	0.964	37.38
GH4/GC-29	15.919	81.914	1048	4	109.53	1.24	2163.24	1882.95	89.69	0.959	20.08
GH4/GC-17	15.877	81.808	1052	3.5	91.58	1.23	1778.57	1563.40	111.48	0.937	15.66
GH4/GC-12	15.796	81.892	1053	0.75	112.99	1.22	2206.07	1904.39	59.13	0.973	25.41
GH4/GC-21	15.892	81.862	1054	3.5	106.65	1.23	2118.48	1857.75	76.88	0.964	19.6
GH4/GC-18	15.858	81.839	1056	3.5	91.24	1.15	1742.60	1533.50	93.41	0.946	22.85
GH4/GC-23	15.901	81.887	1057	3.4	111.52	1.25	2134.10	1836.59	58.76	0.972	21
GH4/GC-30	15.922	81.935	1063	3.5	94.98	1.17	1812.43	1623.23	67.42	0.963	15.68
GH4/GC-70	15.962	81.984	1065	4	114.49	1.20	2221.55	1975.45	88.03	0.960	21.06
GH4/GC-35	15.941	81.959	1070	3.5	109.90	1.23	2103.55	1885.71	67.87	0.968	21.5
GH4/GC-41	15.965	82.010	1077	3.8	89.36	1.09	1614.15	1351.28	60.85	0.962	22
GH4/GC-13	15.810	81.822	1085	2.5	93.97	1.23	1817.86	1657.12	97.50	0.946	24.39
GH4/GC-15	15.886	81.784	1103	3.5	110.31	1.23	2172.09	1979.90	89.98	0.959	21.89
GH4/GC-45	15.989	82.072	1107	4	109.16	1.26	2095.42	1840.51	82.05	0.961	19.57
GH4/GC-46	15.998	82.134	1107	4.1	88.55	1.17	1605.58	1450.71	81.73	0.949	22.99
GH4/GC-62	16.112	82.231	1107	5	136.44	1.21	2694.91	2239.27	90.04	0.967	22.24
GH4/GC-52	16.012	82.170	1114	4	100.76	1.24	1828.12	1645.89	67.20	0.963	19.14
GH4/GC-20	15.857	81.876	1116	4	109.59	1.26	2132.37	1917.14	104.36	0.951	23.84
GH4/GC-54	16.038	82.183	1117	3.7	94.10	1.08	1770.49	1539.76	88.52	0.950	31.01
GH4/GC-24	15.870	81.890	1124	3.3	109.08	1.27	2066.82	1771.78	67.11	0.968	22.24
GH4/GC-40	15.954	82.053	1158	4.5	97.15	1.22	2123.60	1910.28	94.47	0.956	15.93
GH4/GC-36	15.903	81.987	1160	4.5	103.64	1.24	1921.59	1722.79	53.69	0.972	15.97
GH4/GC-37	15.915	82.004	1160	4	101.09	1.23	1936.20	1741.22	98.23	0.949	21.43
GH4/GC-14	15.854	81.803	1181	3.25	97.75	1.19	1909.37	1734.31	69.36	0.964	25.8
GH4/GC-58	16.080	82.233	1197	3.7	103.42	1.19	1983.18	1772.62	98.15	0.951	15.45
GH4/GC-53	16.035	82.203	1202	3.4	110.39	1.27	2116.38	1881.64	92.48	0.956	26.04
GH4/GC-39	15.904	82.065	1218	5.25	104.58	1.23	1968.97	1776.41	90.11	0.954	24.59
GH4/GC-64	16.128	82.279	1222	3.7	98.25	1.14	2009.06	1762.91	103.10	0.949	24.34
GH4/GC-26	15.837	81.927	1230	5	105.63	1.25	2002.88	1794.41	83.84	0.958	28.45
GH4/GC-8	15.840	81.773	1231	3.25	100.50	1.23	2048.40	1821.00	94.66	0.954	31.22
GH4/GC-59	16.053	82.223	1248	2.7	93.71	1.19	1705.23	1349.28	71.33	0.958	22.82
GH4/GC-19	15.833	81.890	1252	3.25	113.90	1.24	2132.74	1799.46	63.17	0.970	18.96
GH4/GC-38	15.884	82.020	1254	4.5	99.40	1.20	1938.90	1760.70	185.76	0.904	16.57
GH4/GC-9	15.792	81.828	1266	4	111.18	1.30	2160.76	1980.58	87.90	0.959	23.45
GH4/GC-10	15.778	81.843	1278	1.8	80.86	1.04	1431.29	1238.70	84.37	0.941	27.79
GH4/GC-27	15.838	81.971	1280	4.5	97.75	1.21	1854.33	1677.36	53.05	0.971	29.5
GH4/GC-60	16.068	82.250	1280	4	94.89	1.22	1768.90	1540.63	70.66	0.960	26.09
GH4/GC-1	15.813	81.730	1327	4.5	123.62	1.21	2428.06	2229.05	84.70	0.965	24.06
GH4/GC-61	16.088	82.280	1332	3.7	92.66	1.19	1755.90	1541.79	77.77	0.956	21
GH4/GC-73	15.802	81.785	1435	5.7	92.66	1.16	1798.61	1677.06	80.58	0.955	28
GH4/GC-11	15.762	81.866	1471	4.3	86.42	1.17	1528.08	1290.29	50.83	0.967	18.97
GH4/GC-7	15.767	81.814	1478	5.25	16.97	0.09	253.23	236.36	55.35	0.781	26.4
GH4/GC-3	15.774	81.759	1500	3	128.79	1.26	2724.25	2480.50	136.50	0.950	26.75
GH4/GC-4	15.773	81.767	1509	3.5	112.89	1.24	2178.03	1949.53	92.70	0.957	22.2
GH4/GC-71	15.775	81.801	1514	5	111.58	1.22	2232.57	2036.93	64.38	0.971	23.74
GH4/GC-72	15.752	81.804	1649	3.3	102.83	1.17	1972.43	1815.31	77.84	0.961	28.44
GH4/GC-5	15.726	81.770	1684	3	116.22	1.20	2458.87	2206.32	83.93	0.966	15.9
GH4/GC-6	15.719	81.800	1745	2.5	110.58	1.22	2331.61	2194.11	118.76	0.949	19.53

Values in bold corresponds to location GC-07.

Table 2

Average surface values and standard deviation for all the available near surface samples in the K-G offshore basin except GC-07. The magnetic anomaly related to GC-07 is also shown for comparison.

Magnetic parameter	Average value (mean)	Std dev	GC-07 anomaly
$X_{LF} \times 10^{-8} \text{ m}^3 \text{ kg}^{-1}$	105	11	17
$X_{FD}\%$	4	0.7	1.4
$X_{ARM} \times 10^{-5} \text{ m}^3 \text{ kg}^{-1}$	1	0.05	0.09
$SIRM \times 10^{-5} \text{ Am}^2 \text{ kg}^{-1}$	2040	279	253
$\text{Soft-IRM} \times 10^{-5} \text{ Am}^2 \text{ kg}^{-1}$	1807	256	236
$\text{Hard-IRM} \times 10^{-5} \text{ Am}^2 \text{ kg}^{-1}$	82	24	55
S-ratio	0.96	0.01	0.78
X_{ARM}/X	12	1	5.5
$SIRM/X \times 10^3$	19	0.85	15

values are observed at shallower depths, and lower values at deeper depths. Susceptibility distribution in the deep ocean basin and on the mounds is rather uniform and shows relatively lower values. The X_{ARM} variation (Fig. 2B) within the slope basin, the NE channel, sedimentary ridges, mounds and the deep ocean basin do not show any pattern with depth. The X_{ARM} variation for the SW channel shows consistent values thereby suggesting a uniform magnetic granulometry (uniform magnetic grain size).

The SIRM (Fig. 3A) variation within the slope basin and the deep ocean basin shows a decreasing trend with increasing water depth, while low values are observed within the deep ocean basin. The SIRM values for the SW channel are independent of water depth, whereas in the NE channel the values decrease with increasing water depth. The SIRM for mounds shows very low and uniform values. Soft-IRM (Fig. 3B) for the slope basin shows a decreasing trend with increasing water depth. Soft-IRM for the SW channel does not show any pattern, whereas the NE channel sediments show a pattern similar to that of the slope basin. The deep ocean basin and mounds are associated with low soft-IRM values.

Hard-IRM (HIRM) values (Fig. 4A) for topmost sediment samples do not show any pattern with respect to geomorphology. S-ratio (Fig. 4B) for the slope basin shows uniform values close to unity, suggesting relative dominance of soft magnetic minerals. The distribution of S-ratio with respect to the NE and SW channels, mounds, sedimentary ridges and deep ocean basin do not reveal any pattern. The lack of HIRM and S-ratio correlation with depth or geomorphology occurs in sharp contrast to the correlation of susceptibility and soft-IRM with depths. The crossplot between HIRM and S-ratio shows that they are highly correlated. We infer that the hard magnetic minerals are not much influenced by the transport processes from the continent.

The X_{ARM}/X (Fig. 5A), a relative magnetic grain size indicator (Banerjee et al., 1981; King et al., 1982), show an increasing trend with respect to the water depth within the slope basin thereby indicating the decrease in magnetic grain size with depth. The NE channel shows a similar pattern of increase in X_{ARM}/X with depth; whereas the SW channel shows no significant pattern. The bathymetry mounds, ocean basin and sedimentary ridges show higher values of X_{ARM}/X suggesting the dominance of fine grain magnetic particles. Magnetic variability of $SIRM/X$ (Fig. 5B) within the slope basin shows uniform values independent of water depth. The mounds and deep ocean basin also shows uniform low $SIRM/X$ values. No pattern is observed for the sedimentary ridges and the two channels. The magnetic variability within the sedimentary ridge does not show any trend or pattern.

The variability of silt (Fig. 6) for all GC cores is published in the National Institute of Oceanography (NIO) technical report (NIO, 2005, Table 1). Silt percentage varies from 15 to 40 with the

mean value of 24 and a standard deviation of 5. In general, the silt fraction of the topmost sediment samples decreases with depth within the slope basin. However, silt variation does not show any pattern in the NE and SW channels. Silt variation for the mounds and deep ocean basin is slightly lower than the average silt fraction within the study region.

To understand the nature of the anomalous magnetic parameters at GC-07, complete downcore variation of magnetic parameters were studied at a sampling interval of 50 cm (Table 3; Fig. 7A–G). Even more depleted values of susceptibility, X_{ARM} , SIRM, soft-IRM and HIRM values were observed downcore. The susceptibility drops to ~1/200th of the average value of the topmost sediment samples. The magnetic extract at GC-07 is small (0.052 wt% of the sediments) as compared to that of nearby topmost sediment samples GC-09 (0.344 wt%) and GC-72 (0.204 wt%). The SEM-EDS analysis of the magnetic extracts confirms the presence of titanomagnetite grains with Ti/Fe ratio varying from 0.3 to 0.65 and titanohematite grains with Ti/Fe ratio varying from 0.8 to unity. The SEM images of magnetic extracts clearly show the dissolution signatures such as itch and pits of a larger titanomagnetite (TM) grains (Fig. 8A,B). A large titanohematite grain also shows a complex dissolution pattern (Fig. 8C). Framboidal pyrite crystals (Fig. 8D) are observed in the magnetic extracts.

5. Discussion

5.1. Magnetic signature at site GC-07 associated with neo-methane flux

One of the interesting observations in the present study is the reduced magnetic susceptibility, X_{ARM} , SIRM, soft-IRM, and HIRM at GC-07 as compared to the corresponding average near surface values of the remaining GC cores. The X , X_{ARM} and SIRM at GC-07 drops to ~1/6th, ~1/4th, and ~1/8th, respectively indicating substantial reduction in the concentration of primary magnetic iron oxide minerals. The X_{ARM}/X , a relative magnetic grain size indicator, is sensitive to stable single domain (SSD) magnetic grains as shown by Banerjee et al. (1981) and King et al. (1982). The anomalously low values of X_{ARM}/X and $X_{ARM}/SIRM$ at GC-07 suggest the absence of SSD magnetic grains and the dominance of pseudo-single domain (PSD)/multi-domain (MD) and/or superparamagnetic (SP) grains. However, the significantly low value of X_{FD} (%) (~1.4) at GC-07 indicates the absence of SP grains. Thus, magnetic properties are primarily governed by PSD/MD grains. The anomalously low S-ratio (0.78), an indicator of magnetic mineralogy (Thompson and Oldfield, 1986; Bloemendal et al., 1988), suggests the presence of high coercive magnetic mineral such as titanohematite. The amount of magnetic extract at GC-07 is anomalously low, approximately 1/4th to 1/6th of the magnetic extract from nearby locations GC-09 and GC-72, further supporting substantial reduction in the concentration of magnetic minerals. The SEM-EDS analysis confirms the presence of titanomagnetite grains (Fig. 8A,B), titanohematite grains (Fig. 8C) and framboidal pyrite crystals (Fig. 8D), and dissolution signatures are clearly observed on the titanomagnetite and titanohematite grains.

In a marine depositional environment, dissolution of magnetic iron oxides occurs due to the decomposition of organic matter. Organic matter oxidation proceeds via multiple pathways involving different organisms and successive use of electron receptors typically in the order O_2 , NO_3^- (under oxic conditions), MnO_2 , Fe_2O_3 , $FeOOH$ (under suboxic conditions), SO_4^{2-} and CO_2 (under anoxic conditions) (Froelich et al., 1979). In suboxic conditions dissolution of magnetic iron oxide occurs due to iron reduction and in anoxic conditions dissolution occurs as a result of sulfidization and pyritization reactions (Canfield and Berner, 1987; Karlin and Levi, 1983,

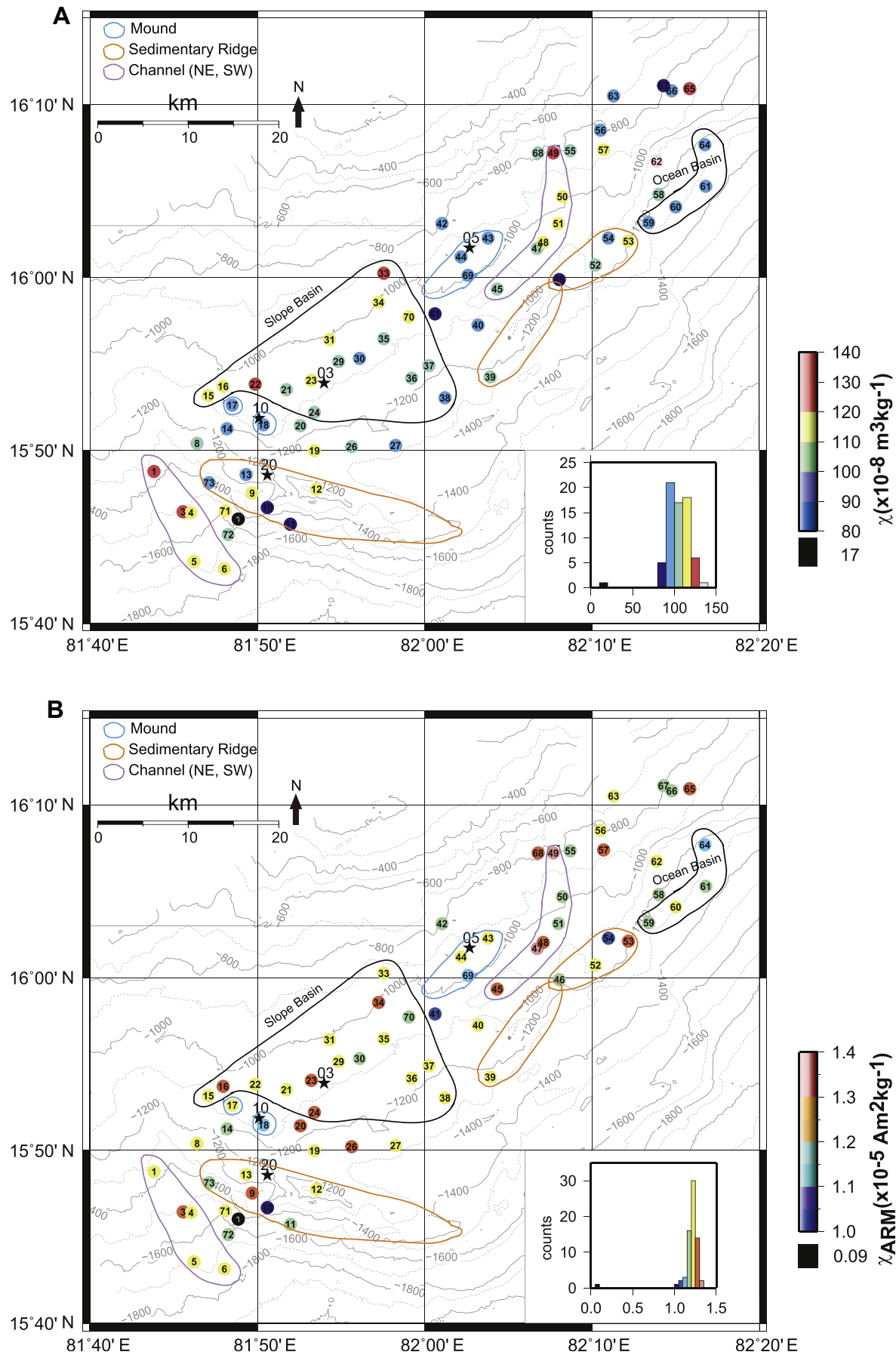


Figure 2. A) Magnetic susceptibility (χ) and B) Susceptibility of ARM (χ_{ARM}) variability with respect to different geomorphologic features. Anomalously low values of susceptibility and χ_{ARM} are observed at GC-07. The insets show the histograms of magnetic susceptibility (A) and χ_{ARM} (B).

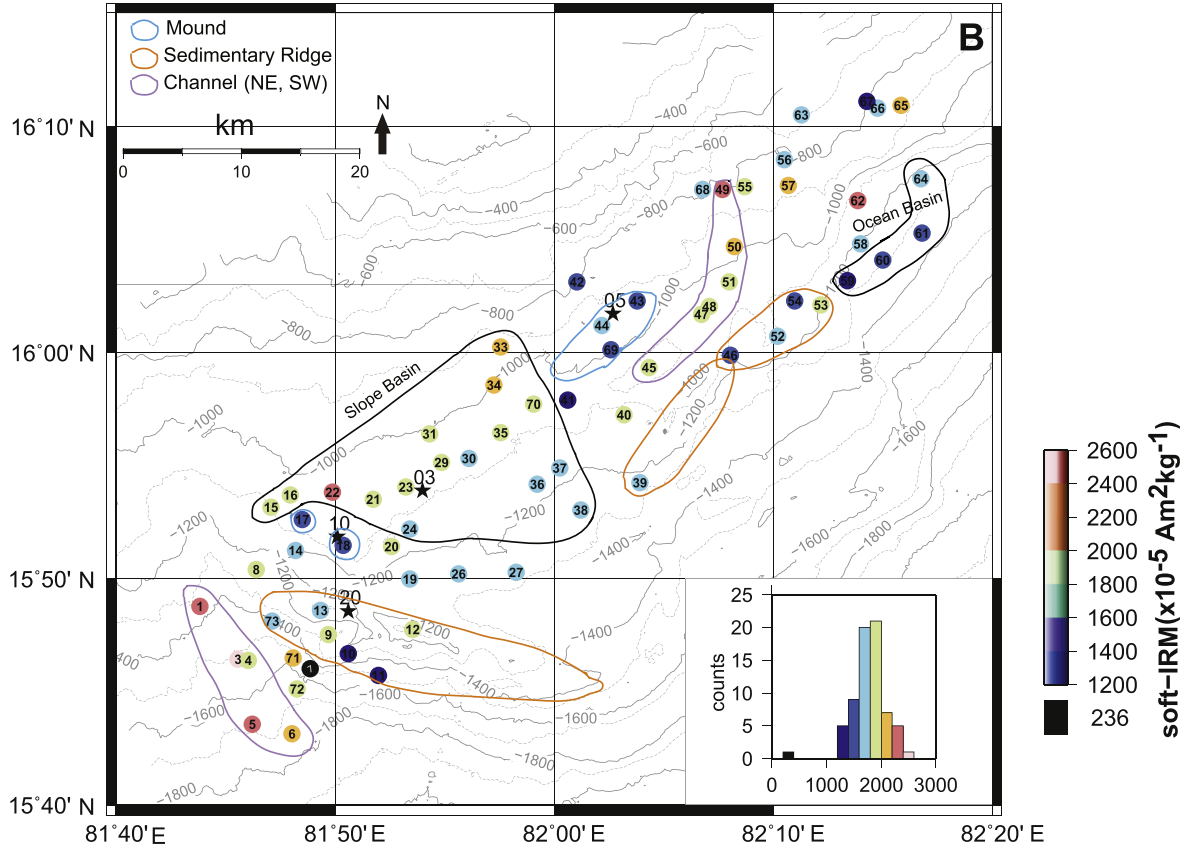
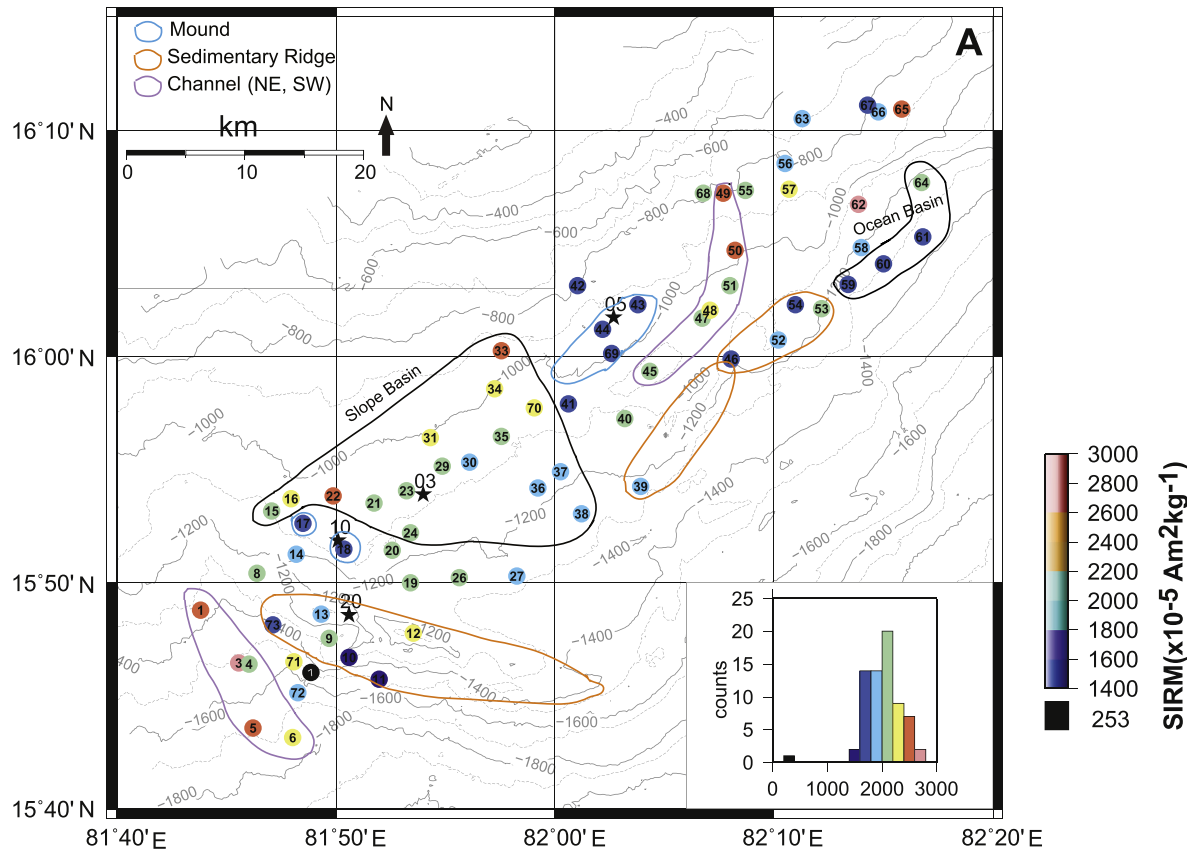


Figure 3. A) SIRM and B) soft-IRM variability with respect to different geomorphologic features. Anomalously low values of SIRM and soft-IRM are observed at GC-07. The insets show the histograms of SIRM(A) and soft-IRM(B).

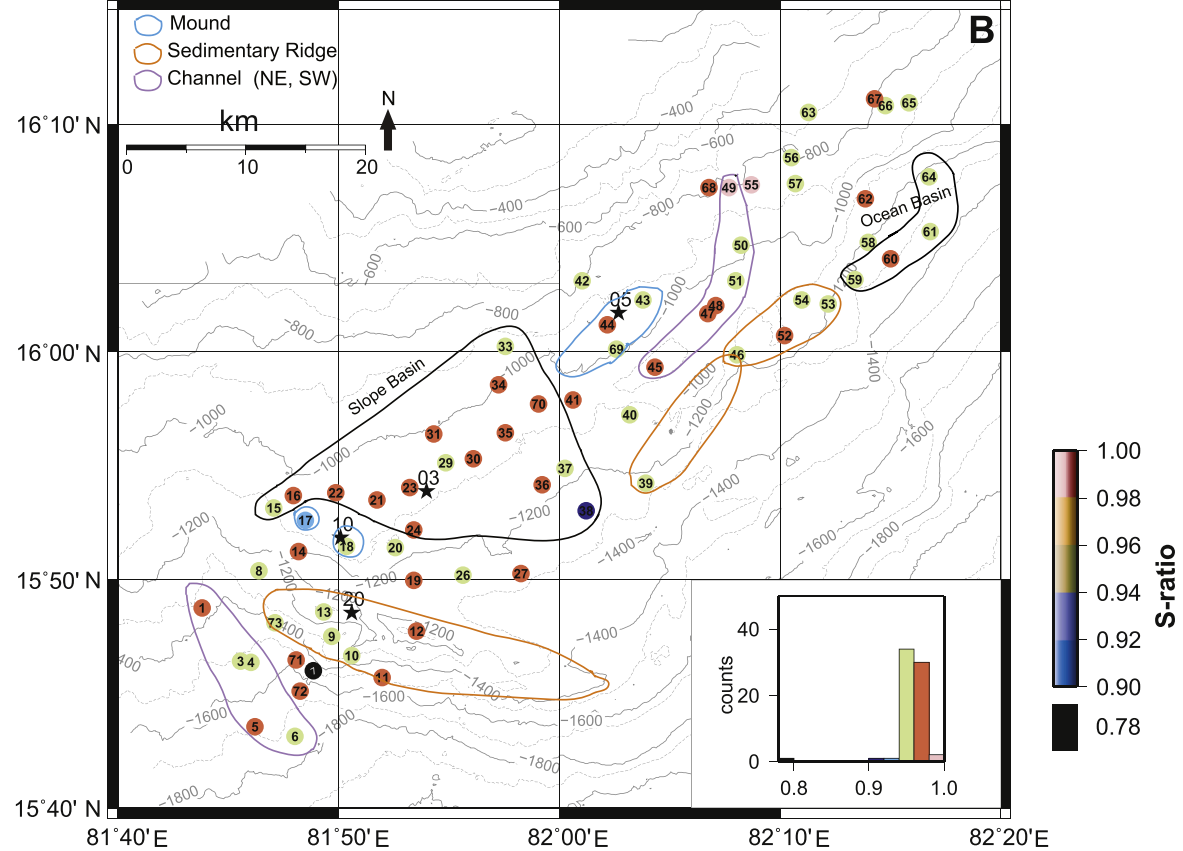
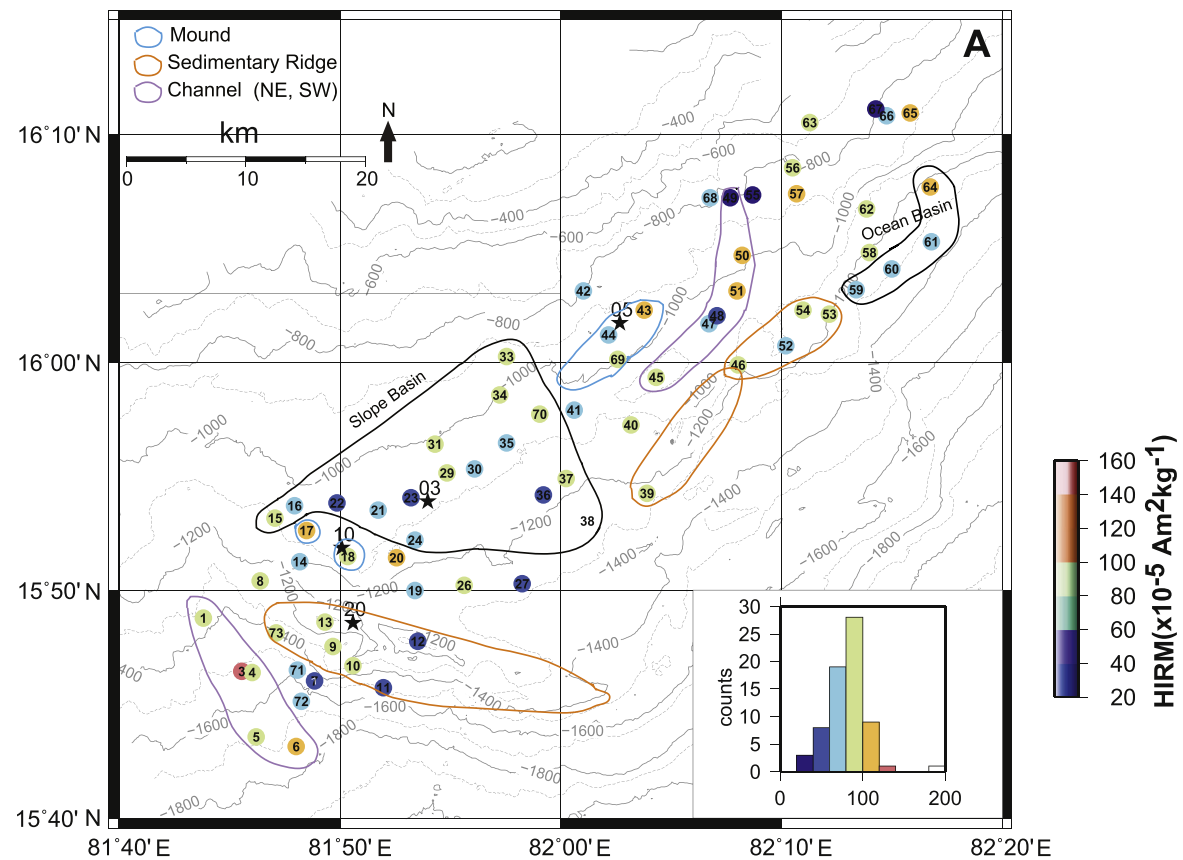


Figure 4. A) HIRM and B) S-ratio variability with respect to different geomorphologic features. Low value of S-ratio is observed at GC-07. The insets show the histograms of HIRM(A) and S-ratio(B).

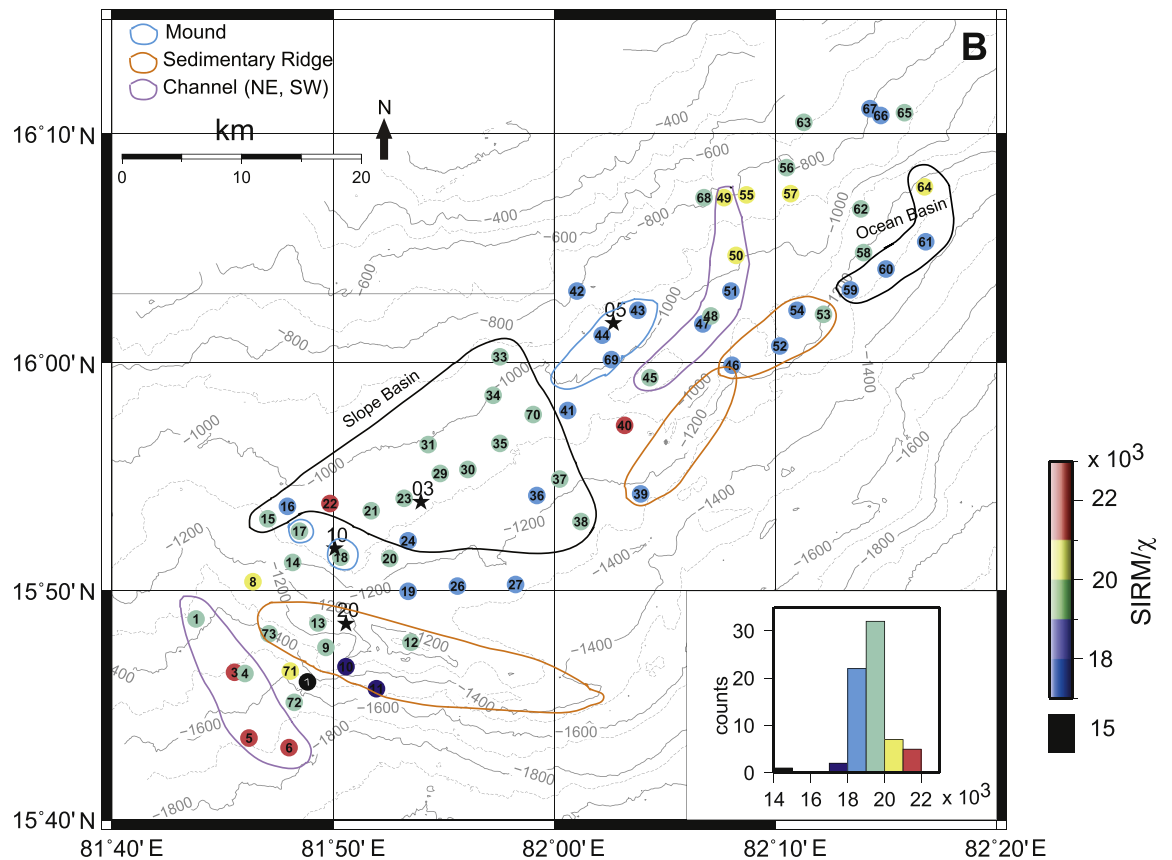
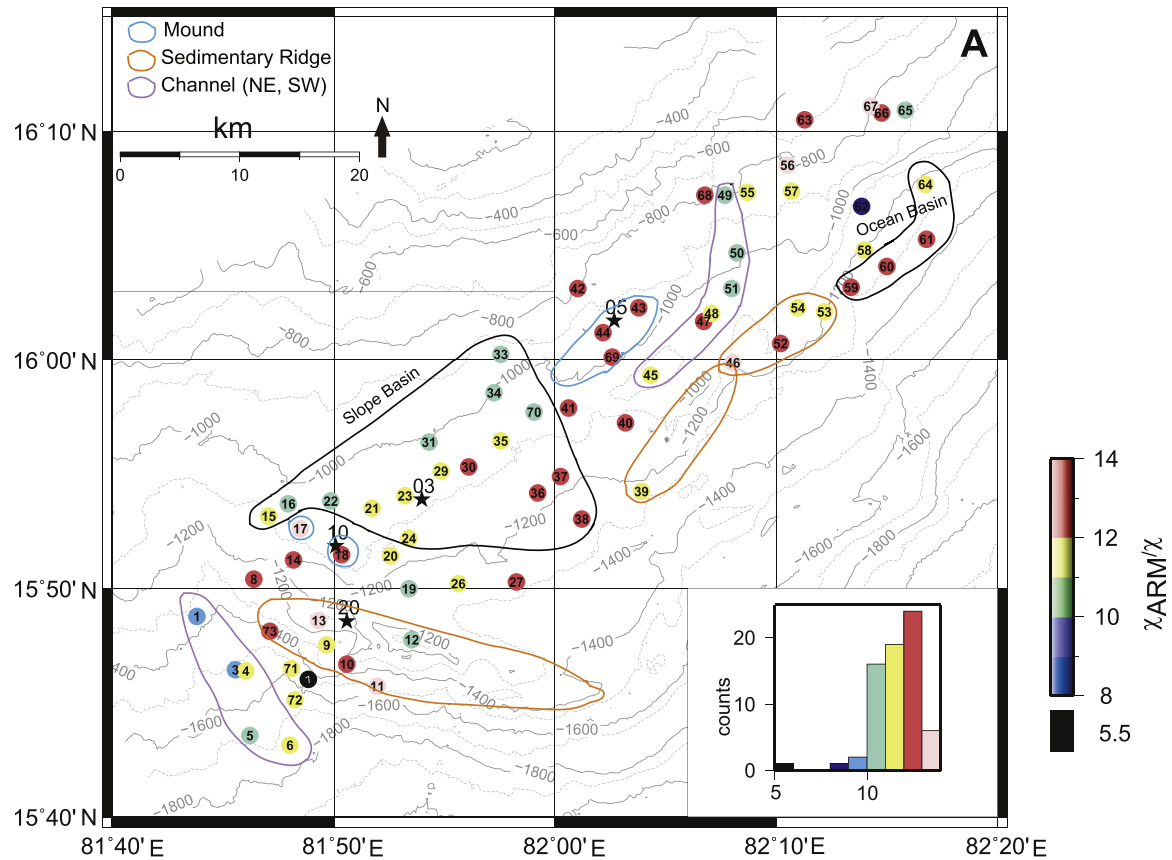


Figure 5. A) X_{ARM}/X and B) $SIRM/X$ variability with respect to different geomorphologic features. Very low X_{ARM}/X and low $SIRM/X$ values are observed at GC-07. The insets show the histograms of X_{ARM}/X (A) and $SIRM/X$ (B).

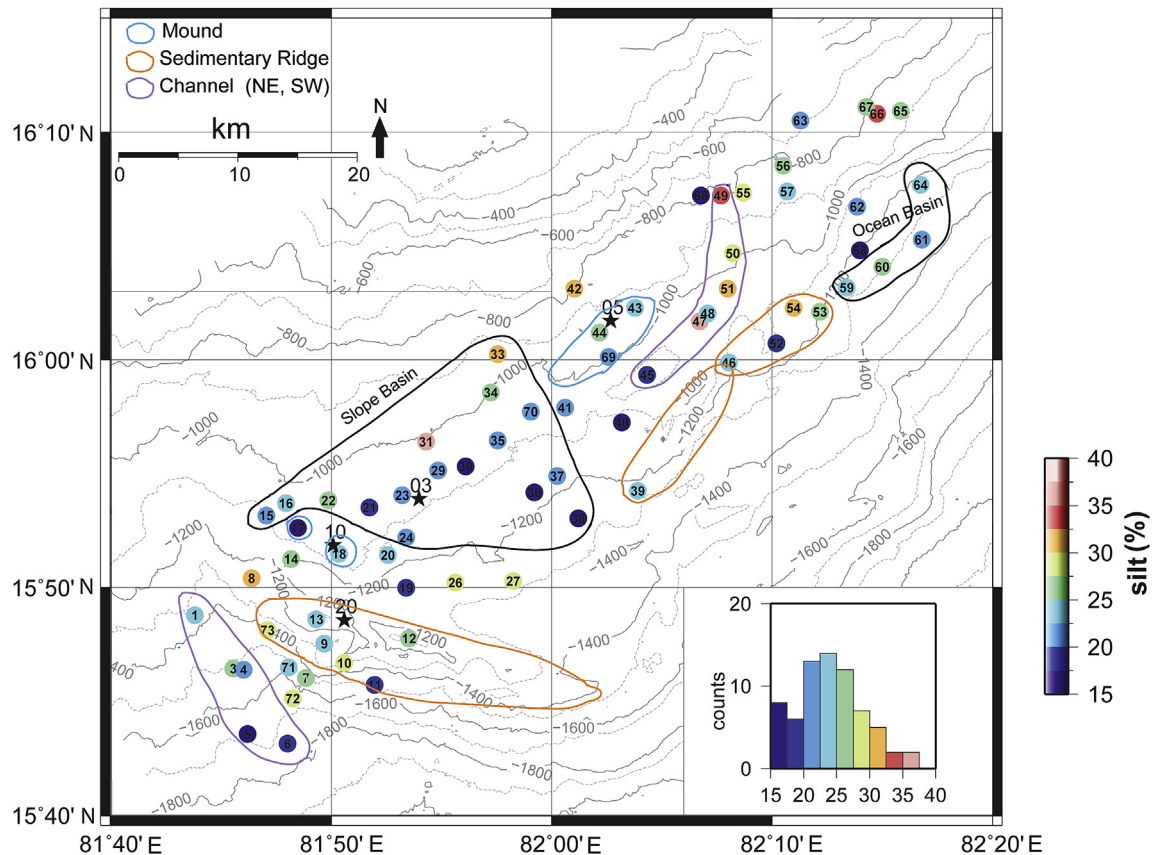


Figure 6. Variability of silt (wt %) with respect to different geomorphologic features in KG offshore basin. The inset shows the histogram of silt.

1985). In addition, anaerobic oxidation of methane (AOM) can rapidly increase the sulphide concentration within the AOM zone (Hensen et al., 2003) leading to enhanced pyritization and increased dissolution of magnetic iron oxide minerals. Thus, the reduced magnetic parameters at GC-07 indicate substantial loss in the concentration of iron oxide mineral phases owing to dissolution driven by iron reduction, organoclastic sulfate reduction and/or AOM.

The core GC-07 is anomalous not only in magnetic properties but also in geological and geochemical properties. The sigmoidal sulfate concentration profile at GC-07 (Fig. 7H, modified after Ramana et al., 2006) shows prominent kinks at 0.9 m below seafloor (mbsf) and 4.2 mbsf suggesting transient or non-steady state pore water chemistry (Hensen et al., 2003; Henkel et al., 2011). In general, the sulfate concentration profiles in the KG offshore basin show linear, concave-up, concave-down, kink-type and quasi-straight type patterns (Mazumdar et al., 2007, 2012).

One of the sulfate concentration profiles (MD161-8) shows a sigmoidal profile similar to that observed at GC-07, and is attributed to the combined influence of sedimentation rate/reactive organic matter burial and enhanced methane flux (Mazumdar et al., 2009, 2012). At MD161-8, the kink observed in the lower part of the sigmoidal profile is interpreted to be due to the upward methane flux. Therefore, we presume that the lower kink (4.2 mbsf) at GC-07 is related to the present day methane flux. The geochemical investigations confirm an abrupt increase in the concentration of dissolved methane (from 3 nM to 153 nM) below 4.2 m of the core (Ramana et al., 2006). Interestingly, none of the other cores depict such prominent increase in the concentration of dissolved methane (NIO, 2005). Further, the sulfate concentration also drops significantly to negligible level at this depth indicating total sulfate reduction primarily due to AOM. AOM is performed by a syntrophic consortium of methanotrophic archaea and sulfate-reducing bacteria (Boetius et al., 2000; Orphan et al., 2001

Table 3

Downcore variation of magnetic parameters at GC-07.

Sample name	Depth cm	Wt gms	X ($\times 10^{-8} \text{ m}^3 \text{ kg}^{-1}$)	X_{HF} ($\times 10^{-8} \text{ m}^3 \text{ kg}^{-1}$)	$X_{\text{FD}} (\%)$	X_{ARM} ($\times 10^{-5} \text{ m}^3 \text{ kg}^{-1}$)	SIRM ($\times 10^5 \text{ Am}^2 \text{ kg}^{-1}$)	Soft-IRM ($\times 10^5 \text{ Am}^2 \text{ kg}^{-1}$)	Hard IRM ($\times 10^5 \text{ Am}^2 \text{ kg}^{-1}$)	S-ratio
25–30	30	4.4914	2.059491	2.058378	0.054054	0.107434	321.4928	260.8174	67.38631	0.790395602
75–80	80	4.83345	1.551687	1.550238	0.093333	0.058711	221.6276	121.5164	64.04105	0.711042057
125–130	130	2.204	1.134301	1.13294	0.12	0.049072	191.0663	82.3329	56.77229	0.702866053
175–180	180	2.1601	0.300912	0.298366	0.846154	0.010424	38.45455	15.55274	9.805935	0.744999379
225–230	230	3.0131	1.145	1.14417	0.072464	0.033436	144.2945	63.15182	38.95517	0.730032025
275–280	280	3.0432	0.755783	0.754798	0.130435	0.023906	104.2763	48.55855	33.41995	0.679505681
325–330	330	2.093	3.081701	3.07979	0.062016	0.055639	244.6501	100.9565	63.18966	0.741714113
425–430	430	4.9588	0.544487	0.544184	0.055556	0.015966	72.45519	40.75201	18.09455	0.75026569
475–480	480	2.7316	1.244692	1.24396	0.058824	0.030194	144.1819	84.1853	29.28002	0.796923107
525–530	530	3.8522	0.558123	0.556695	0.255814	0.02011	85.88737	55.08469	17.21083	0.799611661

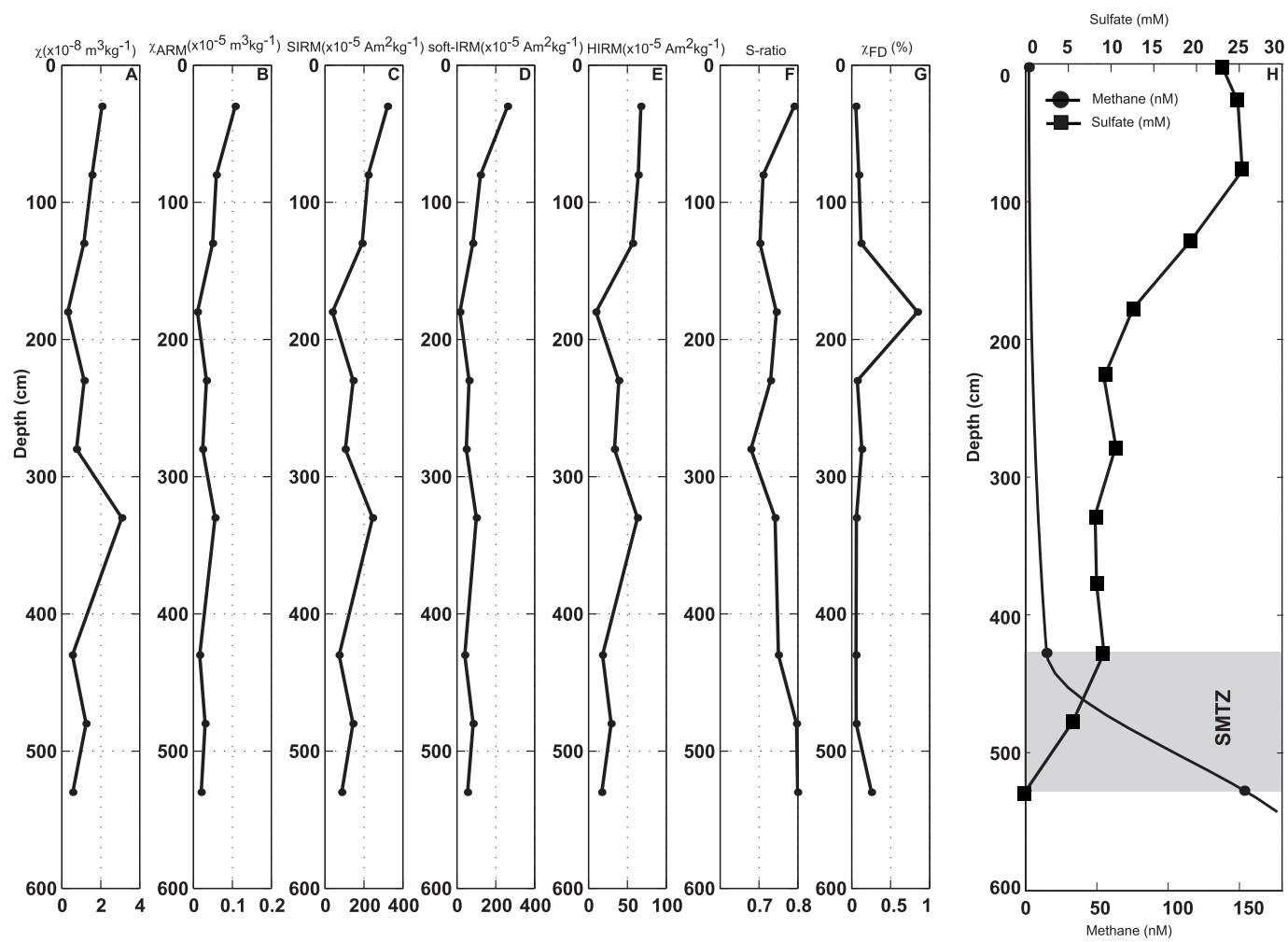


Figure 7. (A–G) Downcore magnetic profile of χ , χ_{ARM} , SIRM, soft-IRM, HIRM, S-ratio, χ_{FD} (%) and H) pore-water geochemistry measurements [Sulfate (mM) and Methane (nM) modified after Ramana et al. (2006)] at GC-07. Sulfate methane transition zone (SMTZ) is observed between 4.2 and 5.2 mbsf.

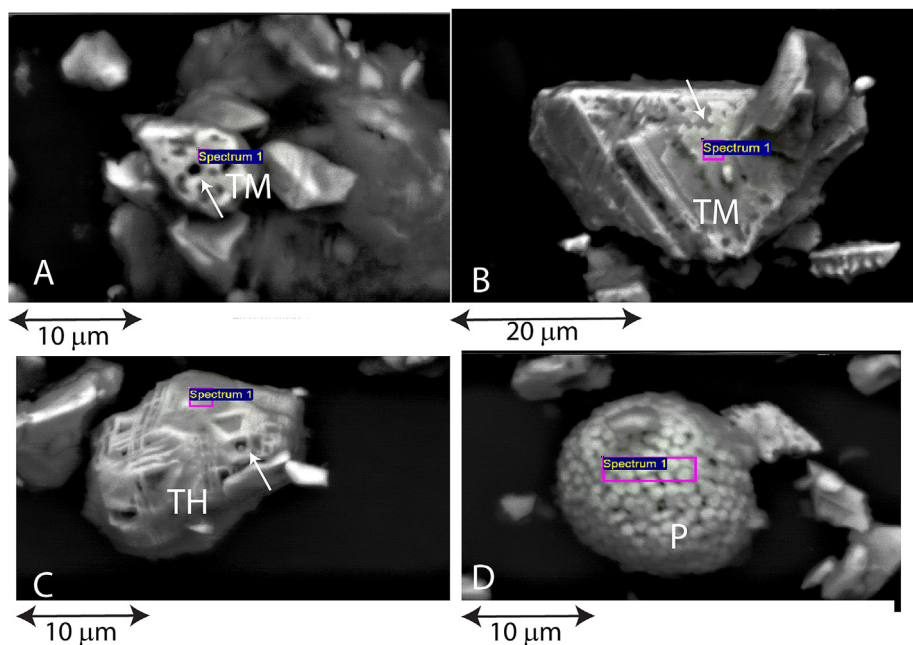
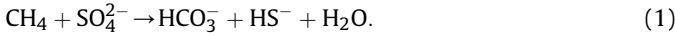
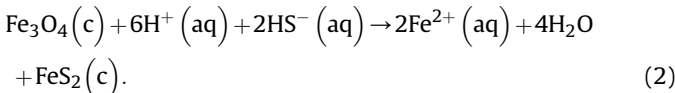


Figure 8. SEM-EDS analysis of magnetic extracts from GC-07. A,B) Dissolution signatures of a larger titanomagnetite (TM) grain; C) complex dissolution pattern of a titanohematite grain (TH); D) a frambooidal pyrite crystal.

Reeburgh, 2007; Knittel and Boetius, 2009). The process can be represented as,



The sulfate–methane transition zone (SMTZ) is defined as the zone within the anoxic sediment column where pore water sulfate and methane concentration profiles intersect. SMTZ occurs between ~4.2 and 5.2 mbsf at GC-07 (Fig. 7H). Likewise, the SMTZ occurs between 15 and 17 mbsf at MD161-8 probably due to lower methane flux (Mazumdar et al., 2009). At GC-07, traces of high-magnesium carbonate with highly depleted carbon isotopic ratios $\delta^{13}\text{C}(\text{‰}) = -51.6$ and $\delta^{18}\text{O}(\text{‰}) = +3.6$ are also observed strongly suggesting that the authigenic carbonates are formed as a result of AOM (Kocherla et al., 2006). Thus, geological and geochemical analyses indicate that site GC-07 is characterized by overall highest upward methane fluxes in the study area. The close association between the upward methane flux and reduced magnetic values at GC-07 suggests that AOM is primarily responsible for the reductive dissolution of magnetic iron oxide minerals as has been demonstrated previously by Riedinger et al. (2005), Novosel et al. (2005) and März et al. (2008). The HS^- released at SMTZ during AOM (eq. (1)) is expected to react with the iron oxides to form stable iron sulfides such as pyrite (Canfield and Berner, 1987) and can be represented as,



It is unlikely that the other processes of iron oxide reduction namely the organoclastic iron reduction and/or the reaction with hydrogen sulfide produced during organoclastic sulfate reduction are responsible for the observed low values of magnetic parameters at GC-07, as these processes are ubiquitous and might have led to widespread occurrence of low magnetic values which are not observed in the present study.

The downcore variation of magnetic parameters at GC-07 further indicates the dissolution of magnetic iron oxide minerals due to AOM. The magnetic susceptibility at SMTZ drops to ~1/200th of the average near surface value indicating almost complete dissolution of magnetic iron oxide minerals. A similar drop in magnetic susceptibility is also observed at 1.8 mbsf in the vicinity of the kink in the sulfate concentration profile. Anomously low values of X_{ARM}/X , $X_{\text{FD}}(\%)$, $X_{\text{ARM}}/\text{SIRM}$ and SIRM/X throughout the core suggest the dominance of coarser PSD/MD grains at GC-07 further supporting the dissolution hypothesis as finer particles dissolve faster than the coarser particles (Karlin and Levi, 1985). The relative increase in the abundance of a high coercive magnetic mineral such as the titanohematite suggests that the low-coercive magnetic mineral (titanomagnetite) dissolves faster than the titanohematite. The continental shelf sediments from the Korea Strait exhibit similar behavior (Liu et al., 2004b). Absence of SP grains as evident from low $X_{\text{FD}}(\%)$ values rules out the possibility of SP domain greigite as observed and explained by Dewangan et al. (2013). Highly depleted X_{ARM}/X and low susceptibility values also rule out the possibility of the presence of SSD greigite. Thus, magnetic susceptibility at GC-07 appears to be controlled either by paramagnetic pyrite, stable end product of the reaction between iron oxide and HS^- (equation (2)), or by coarser PSD/MD grains of titanomagnetite or titanohematite. Novosel et al. (2005), Riedinger et al. (2005), März et al. (2008) and Dewangan et al. (2013) also reported similar reduction in magnetic susceptibility and other magnetic parameters due to HS^- produced by AOM in sediments of the Cascadia accretionary margin, the continental margin off

Argentina and Uruguay, the Zambezi deep-sea fan, and the KG offshore basin, respectively.

The present day sulfate reduction profile at GC-07 leads to dissolution of magnetic iron oxide minerals in the vicinity of SMTZ. The observed dissolution of magnetic iron oxide minerals above the current depth of the SMTZ suggests that either the upward methane flux at site GC-07 was higher in the past or the HS^- is diffusing upward from the current depth of AOM. It is known that the methane flux is variable in the KG basin probably due to the opening and closing of the fault system formed due to neo/shale tectonism (Dewangan et al., 2010; Mazumdar et al., 2012) and may lead to episodic intensification of AOM as demonstrated by Peketi et al. (2012). Therefore, it is likely that the methane flux was enhanced in the past. However, it is difficult to establish the exact mechanism in the absence of HS^- data. Further geological/geochemical investigations are warranted at GC-07 to establish the mechanism of magnetic dissolution due to upward methane flux.

5.2. The variability of magnetic parameters of near surface sediment samples from KG offshore basin

In addition to the magnetic signature associated with methane flux, we made an attempt to understand the distribution of magnetic parameters for various depositional environments in the KG offshore basin. The depositional environments such as slope basin, channels, mounds, sedimentary ridges and deep ocean basin (Fig. 1) are inferred from the analysis of multibeam bathymetry, sub-bottom profiler, high resolution sparker and conventional multi-channel seismic data (Ramana et al., 2006; Dewangan et al., 2010). Any variation/pattern of magnetic parameters within these depositional environments is interpreted in terms of sediment sorting/transport mechanism. Some variability in the magnetic parameters may arise due to differences in the depth of the topmost sediment samples since the magnetic properties are depth dependent owing to reductive dissolution (Canfield and Berner, 1987; Karlin and Levi, 1983, 1985). We assume that such variability is essentially random and may not show any correlation with depth or any other sediment properties.

5.2.1. Slope basin

The slope basin in the study area is characterized by mud flows and sediment buildups associated with mass transport deposits (MTDs) (Ramana et al., 2009; Ramprasad et al., 2011; Dewangan et al., 2010). These MTDs are overlain by a 5–23 m thick, wedge shaped, late Holocene sediment cover (Mazumdar et al., 2012). Therefore, the inferred age of the topmost sediment samples is late Holocene. The titanomagnetite with Ti/Fe ratio of 0.3–0.65 is the dominant detrital magnetic mineral in the study region. Magnetic susceptibility variability within the slope basin decreases systematically with water depth (Fig. 9A). A similar decreasing trend is also observed for SIRM and soft-IRM. In contrast, the X_{ARM}/X values show an increasing trend suggesting the decrease in the abundance of SSD grains. A strong correlation is also observed between SIRM and magnetic susceptibility (Fig. 9B) with a linear regression coefficient of $r^2 = 0.909$ indicating the dominance of detrital ferri-magnetic minerals, as paramagnetic and diamagnetic minerals do not contribute to SIRM (Thompson and Oldfield, 1986). Interestingly, grain size of the topmost sediment samples shows a decreasing trend in silt fraction with increasing water depths. The cross plot between magnetic susceptibility and silt fraction (Fig. 9C) shows good correlation with a linear regression coefficient of $r^2 = 0.61$. These correlations suggest that the magnetic parameters within the slope basin are governed by size and abundance of detrital magnetic minerals (titanomagnetite/titanohematite) which are controlled by the sediment sorting/transport

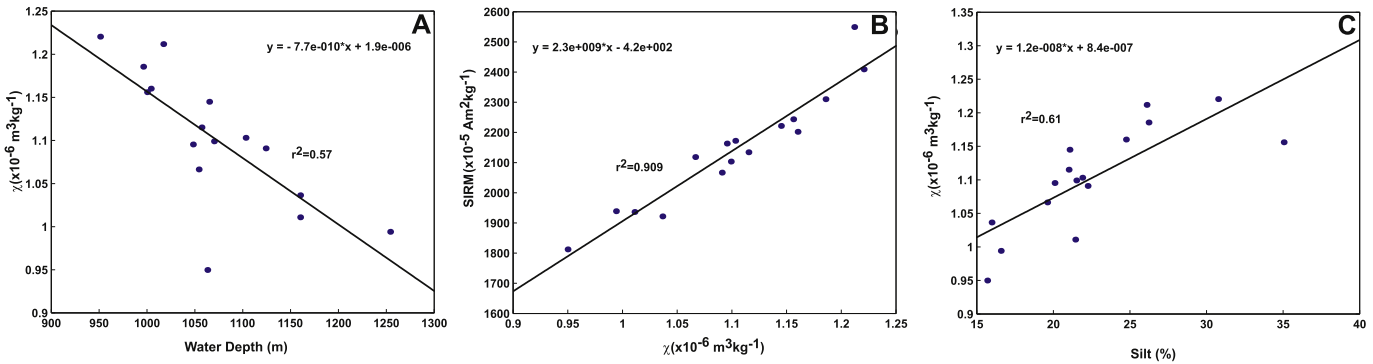


Figure 9. A) Cross plot between X and water depth, B) cross plot between SIRM and X , C) cross plot between X and silt for samples within slope basin.

mechanism. The fine grain particles characterized by low susceptibility and high X_{ARM}/X ratio, settle in deep water while the coarse grains settle in shallow water. Similar correlation between grain size and magnetic susceptibility has been observed in the Loch Lomond drainage basin (Thompson and Morton, 1979), continental shelf sediments of Vancouver Island (Currie and Bornhold, 1983), Changjiang and Huanghe estuaries (Wang et al., 2009), South China sea (Liu et al., 2010) and North Eastern continental shelves of China (Wang et al., 2010).

5.2.2. NE and SW channels

The study area is characterized by two distinct channels, one in the north-east (NE) and the other in south-west (SW) direction (Fig. 1). The SW channel is a linear turbidity channel, bounded by steep scars suggesting high energy depositional environment (cf. Ramana et al., 2009) whereas the NE channel is sinuous with gentle boundaries. Magnetic susceptibility decreases systematically with increasing water depth for both the channels. A decreasing trend is observed in SIRM and soft-IRM values for the NE channel. On the contrary, X_{ARM}/X ratio increases with water depth indicating a systematic decrease in the abundance of SSD grains. These magnetic trends are similar to those observed for the slope basin; hence they represent the sediment sorting/transport process of detrital magnetic minerals. No such pattern is observed for the SW channel suggesting the lack of sorting in this channel which may be related to a high energy environment. Detailed magnetic measurements along with sedimentological data are required to understand the flow process and associated sorting in these channels.

5.2.3. Mounds, deep ocean and sedimentary ridges

The mounds (topographically elevated regions as compared to the surrounding seafloor) show acoustic signatures of fluid/gas migration through the fault/fracture system (Dewangan et al., 2010). These mounds show lower susceptibility, SIRM and soft-IRM values as compared to those of the surrounding region indicating appreciable decrease in the concentration of detrital titanomagnetite grains. Higher values of X_{ARM}/X over the mounds indicate fine grain magnetic particles. The above observations suggest that the topographically elevated regions probably receive lower concentration and fine grain detrital sediments. Likewise, the ocean basin represents a deep offshore region which is expected to be dominated by fine grain sediments. The magnetic signatures associated with the deep ocean are similar to those of mounds, and reflect lower concentration and fine grain detrital magnetic minerals. No confirmed evidence of dissolution is observed in the near surface sediments over the mound despite the presence of sub-surface gas hydrate.

Sedimentary ridges show mixed values in magnetic susceptibility, X_{ARM} , SIRM, and soft-IRM representing high variability in the

concentration and grain size of the magnetic minerals. Furthermore, no pattern is observed in the distribution of the silt fraction. High values of X_{ARM}/X over these ridges suggest the dominance of fine particles as expected in deeper depths. These ridges are affected by frequent slumping/sliding and toe-thrust faulting (Ramana et al., 2007, 2009; Dewangan et al., 2010; Riedel et al., 2010; Ramprasad et al., 2011). Therefore, the high variability in the magnetic parameters may be linked to mixed depositional environment.

6. Conclusion

Magnetic parameters of topmost sediment samples of GC cores from the KG offshore basin have been studied using rock magnetic techniques to identify the magnetic signatures associated with elevated methane flux and to understand the distribution of detrital magnetic minerals vis-à-vis depositional environment. One of the locations, GC-07 shows anomalously low values of X , X_{ARM} and SIRM indicating substantial loss in the concentration of primary magnetic iron oxide minerals. The downcore magnetic profile shows even more depleted values of magnetic parameters. The drop in sulfate concentration and downcore increase in the methane concentration beyond 4.2 mbsf suggest the presence of AOM at GC-07. Therefore, the dissolution of magnetic iron oxide minerals may be attributed to HS^- released due to AOM. The dissolution has preferentially dissolved finer magnetic minerals as indicated by the decrease in the values of X_{ARM}/X and $X_{\text{ARM}}/\text{SIRM}$. The relative abundance of a high coercive mineral such as titanohematite also increases as it is more resistant to dissolution. The observed dissolution of magnetic iron oxide minerals above the current depth of SMTZ suggests enhanced methane flux in the past, and the release of HS^- within paleo-SMTZ might have led to the dissolution. Detailed studies are warranted to further characterize this seep location.

In addition, the variability of magnetic parameters is interpreted in terms of sediment sorting/transport mechanism in the KG offshore basin. The analysis of magnetic parameters within the slope basin and channels shows systematic decrease in magnetic mineral concentration and increase in the abundance of SSD magnetic grains with depth. The strong correlation between the silt fraction and the magnetic susceptibility suggests that the size and concentration of detrital magnetic minerals is predominantly controlled by the sediment sorting/transport mechanism.

Acknowledgments

The author(s) wish to thank those who contributed to the success of the National Gas Hydrate Program Expedition-01 (NGHP-01). NGHP-01 was planned and managed through collaboration

between the Directorate General of Hydrocarbons (DGH) under the Ministry of Petroleum and Natural Gas (India), the U.S. Geological Survey (USGS), and the Consortium for Scientific Methane Hydrate Investigations (CSMHI) led by Overseas Drilling Limited (ODL) and FUGRO McClelland Marine Geosciences (FUGRO). The platform for the drilling operation was the research drill ship JOIDES Resolution, operated by ODL. Much of the drilling/coring equipment used was provided by the Integrated Ocean Drilling Program (IODP) through a loan agreement with the US National Science Foundation. Wireline pressure coring systems and supporting laboratories were provided by IODP/Texas A&M University (TAMU), FUGRO, USGS, U.S. Department of Energy (USDOE) and HYACINTH/GeoTek. Down-hole logging operational and technical support was provided by Lamont-Doherty Earth Observatory (LDEO) of Columbia University. The financial support for the NGHP-01, from the Oil Industry Development Board, Oil and Natural Gas Corporation Ltd., GAIL (India) Ltd. and Oil India Ltd. is gratefully acknowledged. We also acknowledge the support extended by all the participating organizations of the NGHP: MoP&NG, DGH, ONGC, GAIL, OIL, NIO, NIOT, and RIL. The Director of National Institute of Oceanography (NIO) is thanked for his encouragement, support and the permission to publish. Sincere thanks to summer interns of IIT Kharagpur and Areef Sardar for carrying out SEM-EDS analysis. VNJCT fellowship to A. Usapkar is sincerely acknowledged. We would also like to thank the reviewers for providing useful comments/suggestions which have improved the quality of the manuscript. This is NIO contribution no. 5631.

References

- Banerjee, S.K., King, J., Marvin, J., 1981. A rapid method for magnetic granulometry with applications to environmental studies. *Geophys. Res. Lett.* 8, 333–336.
- Basavaiah, N., Khadikar, A.S., 2004. Environmental magnetism and its application towards palaeomonsoon reconstruction. *J. Indian Geophys. Union* 8, 1–14.
- Bastia, R., 2007. Geologic Settings and Petroleum Systems of India's East Coast Offshore Basins: Concepts and Applications. Technology Publications, Dehradun.
- Bloemendal, J., Lamb, B., King, J., 1988. Paleoenvironmental implications of rock-magnetic properties of late Quaternary sediment cores from the eastern equatorial Atlantic. *Paleoceanography* 3, 61–87.
- Boettius, A., Ravenschlag, K., Schubert, C.J., Rickert, D., Widdel, F., Gieseke, A., Amann, R., Jorgensen, B.B., Witte, U., Pfannkuche, O., 2000. A marine microbial consortium apparently mediating anaerobic oxidation of methane. *Nature* 407, 623–626.
- Booth, C.A., Walden, J., Neal, A., Smith, J.P., 2005. Use of mineral magnetic concentration data as a particle size proxy: a case study using marine, estuarine and fluvial sediments in the Carmarthen Bay area, South Wales, U.K. *Sci. Total Environ.* 347, 241–253.
- Canfield, D.E., Berner, R.A., 1987. Dissolution and pyritization of magnetite in anoxic marine sediments. *Geochim. Cosmochim. Acta* 51, 645–659.
- Collett, T.S., Riedel, M., Cochran, J., Boswell, R., Kumar, P., Sathe, A., NGHP Expedition 01 Scientific Party, 2008. Geologic Controls on the Occurrence of Gas Hydrates in the Indian Continental Margin: Results of the Indian National Gas Hydrate Program Expedition 01.
- Collinson, D.W., 1983. Methods in Rock Magnetism and Palaeomagnetism – Techniques and Instrumentation. Chapman Hall, London, 503 pp.
- Currie, R.G., Bornhold, B.D., 1983. The magnetic susceptibility of continental-shelf sediments, west coast Vancouver Island, Canada. *Mar. Geol.* 51, 115–127.
- Dearing, J.A., 2000. Natural magnetic tracers in fluvial geomorphology. In: Foster, I.D.L. (Ed.), Tracers in Geomorphology. John Wiley and Sons, London, pp. 57–82.
- Dewangan, P., Basavaiah, N., Badesab, F.K., Usapkar, A., Mazumdar, A., Joshi, R., Ramprasad, T., 2013. Diagenesis of magnetic minerals in a gas hydrate/cold seep environment off the Krishna-Godavari basin, Bay of Bengal. *Mar. Geol.* 340, 57–70.
- Dewangan, P., Ramprasad, T., Ramana, M.V., Mazumdar, A., Desa, M., Badesab, F.K., 2010. Seabed morphology and gas venting features in the continental slope region of Krishna-Godavari basin, Bay of Bengal: implications in gas-hydrate exploration. *Mar. Pet. Geol.* 27, 1628–1641.
- Donovan, T.J., Forney, R.L., Roberts, A.A., 1979. Aeromagnetic detection of diagenetic magnetite over oil fields. *Am. Assoc. Pet. Geol. Bull.* 63, 245–248.
- Duck, R.W., Rowan, J.S., Jenkins, P.A., Youngs, I., 2001. A multi-method study of bedload provenance and transport pathways in an estuarine channel. *Phys. Chem. Earth Part B Hydrol. Oceans Atmos.* 26, 747–752.
- Ellwood, B.B., Balsam, W.L., Roberts, H.H., 2006. Gulf of Mexico sediment sources and sediment transport trends from magnetic susceptibility measurements of surface samples. *Mar. Geol.* 230, 237–248.
- Esteban, L., Hamilton, T.S., Enkin, R.J., Lowe, C., Novosel, I., 2010. Gas hydrates and magnetism: surveying and diagenetic analysis. In: Riedel, M., Willoughby, E.C. (Eds.), *Gas Hydrates, Geophysical Developments Series*. Society of Exploration Geophysicists, pp. 197–215.
- Fu, Y., von Dobeneck, T., Franke, C., Heslop, D., Kasten, S., 2008. Rock magnetic identification and geochemical process models of greigite formation in Quaternary marine sediments from the Gulf of Mexico (IODP Hole U1319A). *Earth Planet. Sci. Lett.* 275, 233–245.
- Froelich, P.N., Klinkhammer, G.P., Bender, M.L., Luedtke, N.A., Heath, G.R., Cullen, D., Dauphin, P., Hammond, D., Hartman, B., Maynard, V., 1979. Early oxidation of organic matter in pelagic sediments of the eastern equatorial Atlantic: suboxic diagenesis. *Geochim. Cosmochim. Acta* 43 (7), 1075–1090.
- Garming, J.F.L., Bleil, U., Riedinger, N., 2005. Alteration of magnetic mineralogy at the sulfate–methane transition: analysis of sediments from the Argentine continental slope. *Phys. Earth Planet. Interiors* 151, 290–308.
- Geiss, C.E., Banerjee, S.K., 1997. A multi-parameter rock magnetic record of the last glacial–interglacial paleoclimate from south-central Illinois, USA. *Earth Planet. Sci. Lett.* 152, 203–216.
- Henkel, S., Strasser, M., Schwenk, T., Hanebutte, T.J.J., Hüsener, J., Arnold, G.L., Winkelmann, D., Formolo, M., Tomasini, J., Krastel, S., Kasten, S., 2011. An interdisciplinary investigation of a recent submarine mass transport deposit at the continental margin off Uruguay. *Geochem. Geophys. Geosyst.* 12 (8), Q08009. <http://dx.doi.org/10.1029/2011GC003669>.
- Hensen, C., Zabel, M., Pfeifer, K., Schwenk, T., Kasten, S., Riedinger, N., Schulz, H.D., Boetius, A., 2003. Control of sulfate pore-water profiles by sedimentary events and the significance of anaerobic oxidation of methane for the burial of sulfur in marine sediments. *Geochim. Cosmochim. Acta* 67 (14), 2631–2647.
- Hoffmann, V., Knab, M., Appel, E., 1999. Magnetic susceptibility mapping of roadside pollution. *J. Geochem. Explor.* 66, 313–326.
- Hornig, C.S., Chen, K.H., 2006. Complicated magnetic mineral assemblages in marine sediments offshore of southwestern Taiwan: possible influence of methane flux on the early diagenetic process. *Terr. Atmos. Ocean. Sci.* 17, 1009–1026.
- Housen, B.A., Musgrave, R.J., 1996. Rock-magnetic signature of gas hydrates in accretionary prism sediments. *Earth Planet. Sci. Lett.* 139, 509–519.
- Karlin, R., Levi, S., 1983. Diagenesis of magnetic minerals in recent hemipelagic sediments. *Nature* 303 (5915), 327–330.
- Karlin, R., Levi, S., 1985. Geochemical and sedimentological control of the magnetic properties of hemipelagic sediments. *J. Geophys. Res.* 90, 10373–10392.
- Kasten, S., Freudenthal, T., Gingele, F.X., Schulz, H.D., 1998. Simultaneous formation of iron-rich layers at different redox boundaries in sediments of the Amazon deep-sea fan. *Geochim. Cosmochim. Acta* 62, 2253–2264.
- King, J., Banerjee, S.K., Marvin, J., Özdemir, Ö., 1982. A comparison of different magnetic methods for determining the relative grain size of magnetite in natural materials: some results from lake sediments. *Earth Planet. Sci. Lett.* 59, 404–419.
- Knittel, K., Boetius, A., 2009. Anaerobic oxidation of methane: progress with an unknown process. *Annu. Rev. Microbiol.* 63, 311–334.
- Kocherla, M., Mazumdar, A., Karisiddaiah, S.M., Borole, D.V., Rao, B.R., Muralidhar, K., 2006. Evidence of methane derived authigenic carbonates from the sediments of KG basin, eastern continental margin of India. *Curr. Sci.* 91, 318–323.
- Larrañaga, J.C., Gracia, E., Garcés, M., Musgrave, R.J., Piñero, E., Martínez-ruiz, F., Vega, M.E., 2006. Rock magnetic identification of magnetic iron sulfides and its bearing on the occurrence of gas hydrates, ODP LEG 204 (Hydrate Ridge). *Proc. Ocean. Drill. Program Sci. Results* 204, 1–33.
- Larrañaga, J.C., Roberts, A.P., Musgrave, R.J., Gracia, E., Piñero, E., Vega, M., Martínez-ruiz, F., 2007. Diagenetic formation of greigite and pyrrhotite in gas hydrate marine sedimentary systems. *Earth Planet. Sci. Lett.* 261, 350–366.
- Liu, J., Chen, Z., Chen, M., Yan, W., Xiang, R., Tang, X., 2010. Magnetic susceptibility variations and provenance of surface sediments in the South China Sea. *Sediment. Geol.* 230, 77–85.
- Liu, Q., Chan, L., Li, H., Wang, F., Zhang, S., Xia, X., Cheng, T., 2004a. Relationship between magnetic anomalies and hydrocarbon microseepage above the Jingbian gas field, Ordos basin, China. *Am. Assoc. Pet. Geol. Bull.* 88 (2), 241–251.
- Liu, J., Zhu, R., Roberts, A.P., Li, S., Chang, J.H., 2004b. High-resolution analysis of early diagenetic effects on magnetic minerals in post-middle-Holocene continental shelf sediments from the Korea Strait. *J. Geophys. Res. Solid Earth* 109, B03103.
- Liu, Q., Liu, Q., Chan, L., Yang, T., Xia, X., Cheng, T., 2006. Magnetic enhancement caused by hydrocarbon migration in the Mawangmiao oil field, Jianghan basin, China. *J. Pet. Sci. Eng.* 53, 25–33.
- Machel, H.G., Burton, E.A., 1991. Causes and spatial distribution of anomalous magnetization in hydrocarbon seepage environments. *Am. Assoc. Pet. Geol. Bull.* 75, 1864–1876.
- Maher, B.A., Thompson, R., 1995. Paleorainfall reconstructions from pedogenic magnetic susceptibility variations in the Chinese loess and paleosols. *Quat. Res.* 44, 383–391.
- Maher, B.A., Thompson, R., Zhou, L.P., 1994. Spatial and temporal reconstructions of changes in the Asian palaeomonsoon: a new mineral magnetic approach. *Earth Planet. Sci. Lett.* 125, 461–471.
- März, C., Hoffmann, J., Bleil, U., de Lange, G.J., Kasten, S., 2008. Diagenetic changes of magnetic and geochemical signals by anaerobic methane oxidation in sediments of the Zambezi deep-sea fan (SW Indian Ocean). *Mar. Geol.* 255, 118–130.
- Mazumdar, A., Dewangan, P., João, H.M., Peketi, A., Khosla, V.R., Kocherla, M., Badesab, F.K., Joshi, R.K., Roxanne, P., Ramamurthy, P.B., Karisiddaiah, S.M.,

- Patil, D.J., Dayal, A.M., Ramprasad, T., Hawkesworth, C.J., Avanzinelli, R., 2009. Evidence of paleo-cold seep activity from the Bay of Bengal, offshore India. *Geochem. Geophys. Geosyst.* 10, Q06005.
- Mazumdar, A., João, H.M., Peketi, A., Dewangan, P., Kocherla, M., Joshi, R.K., Ramprasad, T., 2012. Geochemical and geological constraints on the composition of marine sediment pore fluid: possible link to gas hydrate deposits. *Mar. Pet. Geol.* 38, 35–52.
- Mazumdar, A., Paropkari, A.L., Borole, D.V., Rao, B.R., Khadge, N.H., Karisiddaiah, S.M., Kocherla, M., João, H.M., 2007. Pore-water sulfate concentration profiles of sediment cores from Krishna–Godavari and Goa basins, India. *Geochem. J.* 41, 259–269.
- Musgrave, R.J., Bangs, N.L., Larrasoña, J.C., Gracia, E., Hollamby, J.A., Vega, M.E., Larrasoña, Juan Cruz, 2006. Rise of the base of the gas hydrate zone since the last glacial recorded by rock magnetism. *Geology* 34, 117–120.
- Neretin, L.N., Böttcher, M.E., Jørgensen, B.B., Volkov, I.I., Lüschen, H., Hilgenfeldt, K., 2004. Pyritization processes and greigite formation in the advancing sulfidation front in the upper Pleistocene sediments of the Black sea. *Geochim. Cosmochim. Acta* 68, 2081–2093.
- NIO, 2005. Geoscientific Investigations of Shallow Sediments in KG Offshore, East Coast. Rep No NIO/TR-13/2003. National Institute of Oceanography, Dona-Paula, Goa.
- Novosel, I., Spence, G.D., Hyndman, R.D., 2005. Reduced magnetization produced by increased methane flux at a gas hydrate vent. *Mar. Geol.* 216, 265–274.
- Oldfield, F., 1991. Environmental magnetism - a personal perspective. *Quat. Sci. Rev.* 10, 73–85.
- Oldfield, F., Maher, B.A., Donoghue, J., Pierce, J., 1985. Particle-size related, mineral magnetic source sediment linkages in the Rhode river catchment, Maryland, USA. *J. Geol. Soc. Lond.* 142, 1035–1046.
- Orphan, V.J., House, C.H., Hinrichs, K.-U., McKeegan, K.D., DeLong, Edward, F., 2001. Methane-consuming archaea revealed by directly coupled isotopic and phylogenetic analysis. *Science* 293, 484–487.
- Peketi, A., Mazumdar, A., Joshi, R.K., Patil, D.J., Srinivas, P.L., Dayal, A.M., 2012. Tracing the Paleo sulfate-methane transition zones and H2S seepage events in marine sediments: an application of C-S-Mo systematic. *Geochem. Geophys. Geosyst.* 13, Q10007. <http://dx.doi.org/10.1029/2012GC004288>.
- Petrovský, E., Kapička, A., Jordanova, N., Knab, M., Hoffmann, V., 2000. Low-field magnetic susceptibility: a proxy method of estimating increased pollution of different environmental systems. *Environ. Geol.* 39, 312–318.
- Powell, C.M., Roots, S.R., Veevers, J.J., 1988. Pre-breakup continental extension in east Gondwanaland and the early opening of the eastern Indian Ocean. *Tectonophysics* 155, 261–283.
- Prabhakar, K.N., Zutshi, P.L., 1993. Evolution of southern part of Indian east coast basins. *J. Geol. Soc. India* 41, 215–230.
- Ramana, M.V., Nair, R.R., Sarma, K.V.L.N.S., Ramprasad, T., Krishna, K.S., Subrahmanyam, V., D'Cruz, M., Subrahmanyam, C., Paul, J., Subrahmanyam, A.S., Sekhar, D.V.C., 1994. Mesozoic anomalies in the Bay of Bengal. *Earth Planet. Sci. Lett.* 121, 469–475.
- Ramana, M.V., Ramprasad, T., Desa, M., Sathe, A.V., Sethi, A.K., 2006. Gas hydrate-related proxies inferred from multidisciplinary investigations in the India offshore areas. *Curr. Sci.* 91, 183–189.
- Ramana, M.V., Ramprasad, T., Kamesh Raju, K.A., Desa, M., 2007. Occurrence of gas hydrates along the continental margins of India, particularly the Krishna–Godavari offshore basin. *Int. J. Environ. Stud.* 64, 675–693.
- Ramana, M.V., Ramprasad, T., Paropkari, A.L., Borole, D.V., Rao, B.R., Karisiddaiah, S.M., Desa, M., Kocherla, M., João, H.M., Lokabharati, P., Gonsalves, M.J., Pattan, J.N., Khadge, N.H., Prakash Babu, C., Sathe, A.V., Kumar, P., Sethi, A.K., 2009. Multidisciplinary investigations exploring indicators of gas hydrate occurrence in the Krishna–Godavari basin offshore, east coast of India. *Geo-Mar. Lett.* 29, 25–38.
- Ramprasad, T., Dewangan, P., Ramana, M.V., Mazumdar, A., Karisiddaiah, S.M., Ramya, E.R., Sriram, G., 2011. Evidence of slumping/sliding in Krishna–Godavari offshore basin due to gas/fluid movements. *Mar. Pet. Geol.* 28, 1806–1816.
- Rao, G.N., 2001. Sedimentation, stratigraphy, and petroleum potential of Krishna–Godavari basin, east coast of India. *Am. Assoc. Pet. Geol. Bull.* 85, 1623–1643.
- Reeburgh, W.S., 2007. Oceanic methane biogeochemistry. *Chem. Rev.* 107, 486–513.
- Reynolds, R.L., King, J.W., 1995. Magnetic records of climate change. *Rev. Geophys.* 33, 101–110.
- Riedel, M., Collett, T.S., Kumar, P., Sathe, A.V., Cook, A., 2010. Seismic imaging of a fractured gas hydrate system in the Krishna–Godavari basin offshore India. *Mar. Pet. Geol.* 27, 1476–1493.
- Riedel, M., Novosel, I., Spence, G.D., Hyndman, R.D., Chapman, R.N., Solem, R.C., Lewis, T., 2006. Geophysical and geochemical signatures associated with gas hydrate-related venting in the northern Cascadia margin. *Geol. Soc. Am. Bull.* 118, 23–38.
- Riedinger, N., Pfeifer, K., Kasten, S., Garming, J.F.L., Vogt, C., Hensen, C., 2005. Diagenetic alteration of magnetic signals by anaerobic oxidation of methane related to a change in sedimentation rate. *Geochim. Cosmochim. Acta* 69, 4117–4126.
- Roberts, A.P., Liu, Q., Rowan, C.J., Chang, L., Carvallo, C., Torrent, J., Horng, C.S., 2006. Characterization of hematite (α -Fe₂O₃), goethite (α -FeOOH), greigite (Fe₃S₄), and pyrrhotite (Fe₇S₈) using first-order reversal curve diagrams. *J. Geophys. Res.* 111, B12S35.
- Rowan, C.J., Roberts, A.P., 2006. Magnetite dissolution, diachronous greigite formation, and secondary magnetizations from pyrite oxidation: unravelling complex magnetizations in neogene marine sediments from New Zealand. *Earth Planet. Sci. Lett.* 241, 119–137.
- Rotman, R., Naylor, L., McDonnell, R., MacNiocaill, C., 2008. Sediment transport on the Freiston shore managed realignment site: an investigation using environmental magnetism. *Geomorphology* 100, 241–255.
- Schumacher, D., 1996. Hydrocarbon-induced alteration of soils and sediments. In: Schumacher, D., Abrams, M.A. (Eds.), *Hydrocarbon Migration and its Near-surface Expression*, American Association of Petroleum Geologists Memoir 66, pp. 71–89.
- Scotese, C.R., Gahagan, L.M., Larson, R.L., 1988. Plate tectonic reconstructions of the Cretaceous and Cenozoic ocean basins. *Tectonophysics* 155, 27–48.
- Tang, Y., Jia, J., Xie, X., 2003. Records of magnetic properties in Quaternary loess and its paleoclimatic significance: a brief review. *Quat. Int.* 108, 33–50.
- Thompson, R., Battarbee, R.W., O'Sullivan, P.E., Oldfield, F., 1975. Magnetic susceptibility of lake sediments. *Am. Soc. Limnol. Oceanogr.* 20, 687–698.
- Thompson, R., Maher, B.A., 1995. Age models, sediment fluxes and palaeoclimatic reconstructions for the Chinese loess and palaeosol sequences. *Geophys. J. Int.* 123, 611–622.
- Thompson, R., Morton, D.J., 1979. Magnetic susceptibility and particle-size distribution in recent sediments of the Loch Lomond drainage basin, Scotland. *J. Sediment. Res. (Petrol.)* 49, 0801–0812.
- Thompson, R., Oldfield, F., 1986. *Environmental Magnetism*. Allen and Unwin, London.
- Tucker, M., 1988. *Techniques in Sedimentology*. Blackwell Scientific Inc., 408 pp.
- Walden, J., Slattery, M.C., Burt, T.P., 1997. Use of mineral magnetic measurements to fingerprint suspended sediment sources: approaches and techniques for data analysis. *J. Hydrol.* 202, 353–372.
- Wang, Y., Dong, H., Li, G., Zhang, W., Oguchi, T., Bao, M., Jiang, H., Bishop, M.E., 2010. Magnetic properties of muddy sediments on the northeastern continental shelves of China: implication for provenance and transportation. *Mar. Geol.* 274, 107–119.
- Wang, Y., Yu, Z., Li, G., Oguchi, T., He, H., Shen, H., 2009. Discrimination in magnetic properties of different-sized sediments from the Changjiang and Huanghe estuaries of China and its implication for provenance of sediment on the shelf. *Mar. Geol.* 260, 121–129.
- Zhong, C., Wen, Y., Xianzan, T., Jianguo, L., Muhong, C., Huaping, Y., 2009. Magnetic susceptibility in surface sediments in the southern south China Sea and its implication for sub-sea methane venting. *J. Earth Sci.* 20, 193–204.